Atmospheric tropical modes are important drivers of Sahelian springtime heatwaves

Climate Dynamics
https://doi.org/10.1007/s00382-020-05569-9

Atmospheric tropical modes are important drivers of Sahelian springtime heatwaves

Kiswendsida H. Guigma[1] · Françoise Guichard[2] · Martin Todd[1] · Philippe Peyrille[2] · Yi Wang[1]

Received: 25 July 2020 / Accepted: 4 December 2020

Abstract
Heatwaves pose a serious threat to human health worldwide but remain poorly documented over Africa. This study uses mainly the ERA5 dataset to investigate their large-scale drivers over the Sahel region during boreal spring, with a focus on the role of tropical modes of variability including the Madden–Julian Oscillation (MJO) and the equatorial Rossby and Kelvin waves. Heatwaves were defined from daily minimum and maximum temperatures using a methodology that retains only intraseasonal scale events of large spatial extent. The results show that tropical modes have a large influence on the occurrence of Sahelian heatwaves, and, to a lesser extent, on their intensity. Depending on their convective phase, they can either increase or inhibit heatwave occurrence, with the MJO being the most important of the investigated drivers. A certain sensitivity to the geographic location and the diurnal cycle is observed, with nighttime heatwaves more impacted by the modes over the eastern Sahel and daytime heatwaves more affected over the western Sahel. The examination of the physical mechanisms shows that the modulation is made possible through the perturbation of regional circulation. Tropical modes thus exert a control on moisture and the subsequent longwave radiation, as well as on the advection of hot air. A detailed case study of a major event, which took place in April 2003, further supports these findings. Given the potential predictability offered by tropical modes at the intraseasonal scale, this study has key implications for heatwave risk management in the Sahel.

Keywords Heatwaves · Tropical modes · Sahel · Drivers · Intraseasonal

1 Introduction

The Sahel is a tropical semi-arid region located in West Africa that experiences high temperatures during the largest part of the year (Nicholson 2018), and especially in spring (March–June, MAMJ). Recent studies (Fontaine et al. 2013; Ringard et al. 2016; Moron et al. 2016; Oueslati et al. 2017; Guichard et al. 2017; Barbier et al. 2018) have highlighted an increase of extreme temperatures, and future projections predict even worse heatwave conditions (Russo et al. 2016; Dosio 2017; Déqué et al. 2017; Xu et al. 2020; Raymond et al. 2020).

Unfortunately, this region is also one of the least economically developed in the world (e.g. Davidson et al. 2003; Tschakert 2007), implying high levels of vulnerability. An efficient way of using the limited resources available to mitigate heatwave impacts, is to focus on preventive actions, based on skilful forecasts of these hazards as already implemented in other places (e.g. WMO N°1142; Wilkinson et al. 2018). The prevention however requires knowledge and understanding of the large-scale drivers of Sahelian heatwaves, which are both currently under-documented.

Greenhouse effect of moisture, hot air advection and incoming solar radiation (at daytime) appear as the dominant processes inducing extremely hot temperatures in spring over the Sahel (e.g. Slingo et al. 2009; Guichard et al. 2009; Oueslati et al. 2017; Guigma et al. 2020). The spring season also marks the peak of monsoon convection over the Guinean region of West Africa (i.e. south of 10° N; Nguyen et al. 2011), and, although not intuitive, there are potential links between convection and Sahelian

Supplementary Information The online version contains supplementary material available athttps://doi.org/10.1007/s00382-020-05569-9.

✉ Kiswendsida H. Guigma
k.guigma@sussex.ac.uk

[1] University of Sussex, Brighton, UK

[2] Centre National de Recherches Météorologiques (CNRS) / Météo-France UMR 3589 Toulouse, Haute Garonne, France

Published online: 23 December 2020

heatwaves. Guigma et al. (2020) indeed found that large-scale heatwaves over the eastern Sahel are associated with a low-level cyclonic circulation anomaly over northern tropical Africa with a decrease of precipitation over the Guinean band, versus an anticyclonic circulation anomaly and an increase of Guinean precipitation for heatwaves over the western Sahel. When convection is weakened over the Guinean band, the associated northeasterly flow indeed allows the transport of hot air from the eastern Sahel/Sahara towards the coast of the western Sahel; conversely, a convective intensification conveys moisture from the Gulf of Guinea into the Sahel, through northward penetration of monsoon flow (e.g. Lothon et al. 2008; Couvreux et al. 2010), leading to longwave warming.

At the synoptic and intraseasonal scale, the Guinean convection is strongly modulated by tropical modes of variability, namely the Madden Julian Oscillation (MJO) and equatorial waves (e.g. Gu 2009; Kamsu-Tamo et al. 2014; Berhane et al. 2015). Can these modes of convective variability by extension modulate heatwaves in the Sahel? This is a plausible scenario in view of previous studies over West Africa. Moron et al. (2018a) for instance, using a weather type approach, found a significant modulation of near surface temperature over northern tropical Africa by the MJO and equatorial Kelvin (EK) waves at the intraseasonal scale in spring. Advection of both hot air and moisture plays an important role in this modulation. Kalapureddy et al. (2010) also found that the synoptic variability over the Sahel, during the pre- (April–June) and post-monsoon (October and November) seasons, is controlled by monsoon surges with a periodicity similar to that of the African Easterly Waves (AEWs; 3–5 days). Furthermore, Couvreux et al. (2010) indicated that these surges can be stationary or westward moving, along with the AEWs. In the same logic, Mera et al. (2014) showed that synoptic and subseasonal circulation disturbances, driven by extratropical cyclones and also by EK and equatorial Rossby (ER) waves, and possibly by the MJO, lead to influx of moisture from the Gulf of Guinea into the Sahel.

Connections between heatwaves and atmospheric synoptic and intraseasonal modes of convective variability have already been evidenced in other regions. Murari et al. (2016), for example, found that the delay of the Indian monsoon onset weakens southwesterlies in the Arabian Sea, favouring clear sky days over India, and subsequently longer lasting and warmer heatwaves. In South America, the intraseasonal variability considerably modulates heatwaves in association with the Southern Atlantic Convergence Zone (Cerne and Vera 2011). In the southeastern part of Australia, Parker et al. (2014) showed that warm conditions are significantly associated with the phases 3–6 of the MJO. More recently, the summer 2018 long lasting heatwave over Northeast Asia was found by Hsu et al. (2020) to have been favoured by an unusually strong MJO over the western Pacific warm pool.

The present research aims at assessing the extent to which and in what ways Sahelian heatwaves are modulated by tropical modes during the MAMJ season. The reason for the focus on tropical modes is the potential for predictability at intraseasonal lead times. Tropical modes are indeed good sources of predictability at these scales (Moron et al. 2018b; Dias et al. 2018; Bengtsson et al. 2019; Li and Stechmann 2020; Judt 2020).

To the best of the authors' knowledge, this study is the first to use a systematic and comprehensive approach to investigate the impact of tropical modes on actual heatwaves in the Sahel. Two complementary methods are used for this purpose. The first consists of a statistical study over the 1979–2018 period while the second exemplifies the emerging overall processes with a detailed case study event in April 2003.

The rest of the manuscript is structured as follows. The data and the methods used are summarised in Sect. 2. Then, Sect. 3 presents the results obtained from the statistical study. In Sect. 4, the case study of the 2003 heatwave event is analysed in detail. Finally, conclusions and perspectives are given in Sect. 5.

2 Methodology

The Sahel area is hereafter defined as the continental domain limited by the coordinates 20° W, 30° E, 10° N, 20° N. Since this work aims at depicting the large-scale drivers, the analysis however extends to the entire northern half of Africa, and sometimes to an even larger domain.

2.1 Data

The main dataset used in this paper is the fifth generation of the European reanalyses ERA5 (Hersbach et al. 2020) at a resolution of $0.5° \times 0.5°$, covering the period 1979–2018. The reason for the choice of this dataset is that it likely offers the best representation of near surface meteorological variables (Olauson 2018; Ramon et al. 2019) as well as radiative fields over land (Martens et al. 2020), and provides a comprehensive and self-consistent set of variables for diagnostic analysis.

This dataset is thus used in this research for (i) heatwave detection from daily minimum and maximum temperature at 2 m (hereafter referred to as "Tmin" and "Tmax" respectively), (ii) tropical mode filtering from outgoing longwave radiation (OLR), and (iii) retrieving physical fields to understand the mechanisms of modulation. Previous studies (Oueslati et al. 2017; Barbier et al. 2018) have already shown the good quality of near surface thermal

indices (including Tmin and Tmax) over the Sahel in ERA-Interim of which ERA5 is an improvement. OLR in ERA5 is taken as the negative of the net top-of-atmosphere (TOA) thermal radiation. Wang et al. (2017), Tall et al. (2019), Wright et al. (2020) and Hersbach et al. (2020) assessed radiative fluxes in different products and found that ERA5 shows TOA fluxes (including OLR) that are very consistent with the observed. Using observed OLR data such as the daily interpolated data from the NOAA (Liebmann and Smith 1996) does not significantly alter the results obtained with ERA5 (not shown), making it suitable for the present study.

Some of the physical variables used for analysing the mechanisms of heatwave modulation are directly available from ERA5: temperature, zonal and meridional components of wind, specific humidity, precipitable water and radiation data. As in Oueslati et al. (2017), the surface energy budget is derived from the radiation fields using the following equation:

$$\frac{c_s \Delta T}{\Delta t} = SWR + LWR + SHF + LHF, \quad (1)$$

where SWR is the net shortwave radiation, LWR is the net longwave radiation, SHF is the sensible heat flux, LHF is the latent heat flux and c_s is the surface heat capacity.

Radiative fluxes are hereafter counted positively when directed from the atmosphere to the surface.

Other meteorological variables necessary for understanding the physical mechanisms of heatwave modulation are not directly accessible from ERA5 and are thus derived. These include advection of heat (Eq. 2) and of specific humidity (Eq. 3) which are obtained from the horizontal components of wind speed, temperature and specific humidity:

$$A_T = -\vec{V}\vec{\nabla}T = -u\frac{\partial T}{\partial x} - v\frac{\partial T}{\partial y} \quad (2)$$

$$A_q = -\vec{V}\vec{\nabla}q = -u\frac{\partial q}{\partial x} - v\frac{\partial q}{\partial y} \quad (3)$$

where T is temperature, q specific humidity and $\vec{V}$ horizontal wind which is decomposed into its zonal (u) and meridional (v) components.

All variables of the ERA5 database described in this section are available at an hourly frequency. The radiative variables are extracted as 12-hourly accumulations (0600 UTC to 1800 UTC for daytime and 1800 UTC to 0600 UTC of day + 1 for nighttime) while the others as instantaneous entries at a 03-hourly resolution. For the latter, the daytime value is obtained by averaging over 0900, 1200, 1500 and 1800 UTC and the nighttime value over 2100, 0000, 0300 and 0600 UTC.

For the specific case of the derived variables (heat and moisture advection), they are first computed at the 03-hourly timescale before daily averaging.

In addition to the ERA5 reanalysis, various observational data have been utilised mainly for the case study (Sect. 4). Satellite estimates of radiative surface fields (incoming and outgoing shortwave and longwave radiation) were extracted from the Clouds and Earth's Radiant Energy System (CERES) Synoptic (SYN1deg) Product (Wielicki et al. 1996; Doelling et al. 2013, 2016) at a spatial resolution of 1° × 1° over the time period 2000–2018. The initial 03-hourly temporal resolution was aggregated to a daily frequency. Satellite estimates of precipitable water from the Atmospheric Infrared Sounder (AIRS, Teixeira et al. 2013) aboard NASA's second Earth Observing System polar-orbiting platform was also used for the case study at 1° × 1° spatial grid. Twice-daily data provided by the ascending and descending orbits were averaged to get daily estimates. This dataset runs from 2002 to 2016. To analyse the evolution of precipitation over the case study period, daily rainfall totals from the Global Precipitation Climatology Project (GPCP, Schamm et al. 2014) were used at a resolution of 1° × 1°. Finally observed 2 m temperature and specific humidity data at the Demokeya station in Sudan located at 30.5° E–13.3° N (Ardö 2013) were also investigated. The data cover the 2002–2012 period with a temporal resolution of 30 minutes. This provides a valuable in-situ observation over the eastern Sahel, a data sparse region, where the case study is mainly investigated.

2.2 Heatwavedetection

Among the different definitions of heatwaves (Perkins 2015), a choice has been made on one allowing to capture major, large-scale events occurring over synoptic to intraseasonal scales during the spring season. Tropical modes are indeed planetary-scale disturbances and their effects are more likely to cover extensive areas than smaller isolated areas. Therefore, as in Guigma et al. (2020), Tmin and Tmax data are first 90-day highpass filtered to retain variability on the scales of interest. Then, potential heatwaves are defined at a given grid-point as spells of at least three consecutive days where the daily anomalies of Tmin or Tmax (taken separately) exceed the 90th percentile of the distribution of the corresponding calendar days. The 90th percentile for a given calendar day is derived, similarly to Russo et al. (2014) and Guigma et al. (2020), over a 31-day window centred on that day, to remove noise caused by the relative shortness of the dataset. After this step, to ensure sampling of only absolutely hot events regardless of the period of the year, potential heatwaves sampled on days where the raw data (i.e. data before deriving the anomalies) do not exceed the 75th percentile of their total distribution are discarded (Guigma

et al. 2020). Heatwave intensity is defined, at each grid-cell and for each heatwave day (not event), as the 90-day high-pass filtered anomaly of Tmin (for a nighttime heatwave) or Tmax (for a daytime heatwave) on that day. Next, major large-scale events are defined by adding a minimum spatial extent threshold of 600,000 km^2 using a region growing technique as in Barbier et al. (2018). The outcome is a set of daily binary masks specifying the regions where these large-scale heatwaves occur, providing the final sample of heatwaves analysed in this study.

It should be noted that heatwaves can also be defined from other thermal indices than Tmin and Tmax, taking into account additional environmental variables (moisture, wind, solar radiation) as in Guigma et al. (2020). Only Tmin and Tmax are however retained for this study because of the consistency of the results across these indices (not shown).

2.3 Tropical mode detection

In this study, the expression "tropical modes'' refers to the synoptic and intraseasonal modes of variability of the tropical atmosphere including the MJO and equatorially trapped waves. The MJO is the most important driver of intraseasonal variability of the tropical atmosphere (Madden and Julian 1971, 1972, 1994) and influences the West African Monsoon (e.g. Sossa et al. 2017). In this study, equatorial waves are explored in connection with convection (hence the expression convectively coupled equatorial waves CCEWs). Over West Africa, Kamsu-Tamo et al. (2014) and Schlueter et al. (2019a, b) demonstrated statistically and dynamically that they have an impact on convection. In the present paper, the equatorial waves under investigation are the ER and EK waves. Other waves such as AEWs and mixed Rossby-gravity waves are not included as they are not so active in the region during the season of interest (MAMJ).

Each tropical mode is characterised by a range of wavenumbers, periods and equivalent depths summarised in Table 1. A wavenumber is the number of waves (each wave comprising one ridge and one trough) that it takes to zonally circumscribe the globe. The period of a wave measures the time separating the passage of two consecutive ridges at a given location. As for the equivalent depth, a more complex notion used for ER and EK wave filtering, it refers to the depth of the shallow layer of atmospheric fluid that is required (by theory) to get the appropriate values for the time-varying and horizontal components of their motion (Wheeler and Nguyen 2015).

Tropical modes are detected from the fields of OLR, which is a good proxy for tropical convection (Arkin and Ardanuy 1989), and has been extensively used in tropical mode investigation over West Africa (e.g. Lavender and Matthews 2009; Pearson et al. 2010; Yang et al. 2018). To extract a given mode, the mean and first three harmonics of the OLR annual cycle are first removed to obtain intraseasonal anomalies. Then, the filtering in the wavenumber-frequency space consists of setting to zero any spectral coefficient outside the window corresponding to the mode of interest (Table 1), such that only the relevant coefficients are retained. The "kf_filter" function of the NCAR Command Language (NCL) was used for this operation. The output of the wavenumber-frequency decomposition is thus a three dimensional (time, longitude and latitude) filtered OLR field for each mode. The full explanation of the method can be found in Wheeler and Kiladis (1999) and Kiladis et al. (2006). No decomposition of the input data into asymmetric and symmetric components is done because the area of interest is fully located on one side of the Equator (northern hemisphere), as already done in several previous studies (e.g. Schreck et al. 2011; Lafore et al. 2017).

In order to characterise the daily local activity of each mode, a phase and amplitude are determined as follows. Firstly, the 5° E longitude (centre of the Sahel domain) is arbitrarily set as reference longitude. Minor variations of the reference longitude do not significantly impact the results (not shown). Then, the daily mode-filtered OLR data at this longitude are averaged over the Guinean zone, i.e. for the latitudes between the Equator and 10°N (vertical line in Fig. 1), where convection is the most active in spring (Nguyen et al. 2011). Including latitudes up to 20° N does not make significant changes to the results. As in Riley et al. (2011), the resulting unidimensional timeseries and its (first order) local time derivative (both normalised by their respective standard deviations) are used to derive the trigonometric form of the corresponding mode, from which an angle and an amplitude are extracted for each day. On a given day, a mode is considered active only if its amplitude is greater than one.

Table 1 Characteristics of each mode used in this study

Mode	Wavenumber band	Period band (days)	Equivalent depth (m)	References
MJO	0–9	20–100	Not specified	Kiladis et al. (2005)
ER	−10 to −1	9.7–72	1–90	Kiladis et al. (2009)
EK	1–14	2.5–20	8–90	Straub and Kiladis (2002), Mekonnen et al. 2008)

The definition of each characteristic is given in Sects. 2, 3

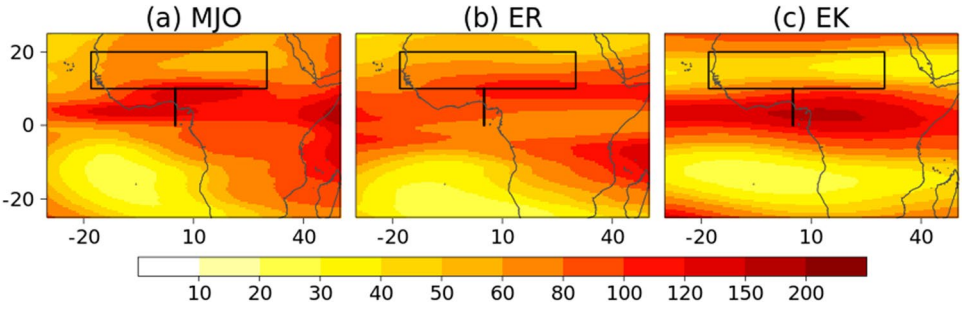

Fig. 1 Variance (in $W^2\ m^{-4}$) of mode-filtered OLR data during MAMJ. The rectangular box delimits the Sahel region. The vertical line marks the reference longitude (5° E) and latitudinal band over which the local activity of tropical modes is characterised (see Sect. 2.3)

Changes to this threshold do not affect the spatial structures of the impact of tropical modes on heatwaves but the magnitude of this impact is slightly modified and is discussed in Sect. 3.3. For the active days of each mode, the angles are further binned into eight 45° wide phases labelled 1–8 such that phase 1 represents instances where the mode is the most convectively suppressed (maximum of OLR), phase 5 the most convectively enhanced (minimum of OLR) and the six others are transitory phases [see the description of the full method in Riley et al. (2011)]. Thus, a given active mode (active because passing the minimum amplitude threshold) can be either in a convectively suppressed or a convectively enhanced phase. It should be noted that, while the practice of setting a reference longitude effectively allows to detect the passage of tropical modes in the region, and to better characterise their local activity, it however comes with the caveat that, away from this longitude, the signal weakens progressively. As a consequence, towards the boundaries of the region, the modes with large wavenumbers are not as well accounted for as those with small wavenumbers.

2.4 Modulation of heatwaves by tropical modes and associated evolution of physical variables

The modulation of heatwave probability of occurrence and heatwave intensity is assessed, during the spring season, by modifying a method initially used by Xavier et al. (2014) for extreme rainfall and Hsu et al. (2017) for heatwaves. It consists of comparing heatwave probability/intensity when a given mode is active on a specific phase versus the climatological probability/intensity during the MAMJ season. The modulation of heatwave probability (MP) is thus given by the following formula:

$$MP = \frac{P_x - P_a}{P_a} \tag{4}$$

where P_x is heatwave probability given the mode is in phase x, i.e. the number of days where heatwaves occur during phase x over the total number of days where the mode is in this phase; P_a is the climatological probability of heatwaves, i.e. the number of heatwave days (regardless of the activity of the modes) over the total number of days. The probabilities are defined in terms of days rather than events, consistently with Hsu et al. (2017).

Likewise, the modulation of heatwave intensity (MI) is defined as follows:

$$MI = \frac{I_x - I_a}{I_a} \tag{5}$$

where I_x is the average heatwave intensity (defined for each heatwave day and at each grid-cell as the highpass filtered anomaly of Tmin or Tmax on that day; Sect. 2.2) given the mode is in phase x and I_a the climatological intensity of heatwaves.

As will be shown in Sect. 3.1, heatwaves can be associated with distinct active tropical modes at different phases, in such a way that the superposition of two modes can lead to an amplified or reduced forcing on heatwaves. The modulation of heatwave probability by two superposed modes is investigated using the following formula:

$$MP = \frac{P_{xy} - P_a}{P_a} \tag{6}$$

P_{xy}: heatwave probability when the first mode is in phase x and the second mode in phase y. P_a: heatwave climatological probability.

The significance of the modulation patterns is tested at each grid-point and for each phase of the modes through bootstrap resampling (Wang et al. 2008; Mazdiyasni and AghaKouchak 2015; Nissan et al. 2017; Harrington et al. 2019). Let N be the number of days where a given mode is in phase × (or one mode in phase × and another in phase y for the superposition case). Then, 1000 random samples, each of size N days are generated. Heatwave probability (or average intensity) is calculated for each sample. From these random probabilities (or average intensities), corresponding values of modulation of heatwave probability (intensity) are derived using Eqs. (4), (5) or (6) accordingly. Significance is finally tested at a 5% probability level against these 1000 random modulation values.

The results of the modulation of heatwave probability are presented in Sect. 3.3, and that of heatwave intensity in Sect. 3.4.

To understand the physical mechanisms associated with the modulation of heatwaves, the composites of each of the diagnostic variables (presented in Sect. 2.1.) are derived over all active mode-phase days. To do this, the mean and the first three harmonics of the seasonal cycle for each variable are first removed. Then, they are passed to a Lanczos highpass filter (Duchon 1979) to retain variability at timescales shorter than 90 days. The filtering causes a loss of data at both edges of the input time series (also observed for heatwave detection and OLR filtering); therefore the analyses cover the 1980–2017 period. Finally, the composite mean of a given variable over a certain instance (e.g. phase × of a mode) corresponds to the average of this variable over all days of this instance. At each grid-point, the significant departure of the average values from zero is tested using the Student's*t* test at the 0.05 probability level. The results are shown in Sect. 3.5.

For the case study purpose, the activity of tropical modes is projected onto various physical fields, similarly to previous studies (e.g. Kiladis et al. 2006; Knippertz and Todd 2010). To do this, the daily mode-filtered OLR data are regressed onto the daily highpass filtered anomalies of the physical variables at each grid-point over the 1980–2017 period. Then, the influence of each tropical mode on the variable during the heatwave event is qualitatively estimated on a daily basis, using the predicted value of the diagnostic variable by the linear regression model. The advantage of this technique is that it allows on a given day to know the likely impact of a certain mode on a physical process (results in Sect. 4.4).

3 Modulation of heatwaves by tropical modes: a statistical analysis

3.1 Activity of tropical modes over Africa during the spring season

Table 2 presents statistics associated with the activity of tropical modes over the Guinean region as detected at the reference longitude of 5° E (described in Sect. 2.3) focusing mainly on the most suppressed and the most enhanced phases (phases 1 and 5 respectively). During the MAMJ season, at least one mode is active 96% of the time irrespectively of the phase. Therefore the spring season is intense in terms of tropical mode activity. For each of these modes, the activity is evenly distributed across the eight phases without a preference for any of them (not shown). The number of active days is not much different from one mode to another but it is apparent that the MJO has the largest sample. The occurrences of exactly one mode (whichever it is) at a given time exclusive of any other mode are quite infrequent (19% of the time). For a given active phase of any mode, merely 10% of its passages satisfy this configuration. Therefore active tropical modes generally overlap. Consequently, an explicit analysis of the impact of these situations on Sahelian heatwaves is undertaken in Sect. 3.3.

The amount of OLR variability explained by the modes is clearly different between them. Figure 1 shows the variance of the mode-filtered anomalies of OLR during the MAMJ season. The MJO, EK and ER waves by decreasing order, have an intense activity over the Guinean sector in boreal spring. For the MJO and EK waves, the variance peaks at above 200 W^2m^{-4} near the Equator (Fig. 1a, c). The MJO is active over the entire sector between 10°S and 15°N. On the other hand, the EK waves are active only within a band surrounding the Equator consistent with theory (the high

Table 2 General statistics associated with the activity of tropical modes at the reference longitude of 5° E

Total number of MAMJ days over the 1980–2017 period	4636
Percentage of days where at least one mode is active	96.5%
Percentage of days where exactly one mode is active	19.0%
Percentage of days where the MJO is active **(and of which EK and ER are inactive)**	72.7% **(9.3%)**
Percentage of days where the ER is active **(and of which MJO and ER are inactive)**	65.7% **(6.6%)**
Percentage of days where the EK is active **(and of which MJO and ER are inactive)**	70.4% **(11.1%)**
Number of days where the MJO is active in phase 5 **(and where ER and EK are inactive)**	409 **(22)**
Number of days where the MJO is active in phase 1 **(and where ER and EK are inactive)**	458 **(41)**
Number of days where the ER is active in phase 5 **(and where MJO and EK are inactive)**	393 **(25)**
Number of days where the ER is active in phase 1 **(and where MJO and EK are inactive)**	409 **(42)**
Number of days where the EK is active in phase 5 **(and where MJO and ER are inactive)**	390 **(40)**
Number of days where the EK is active in phase 1 **(and where MJO and ER are inactive)**	443 **(38)**

See Sect. 3.1 for the analysis

variance of EK waves observed at the edges of the domain are mainly due to imperfections in the filtering technique which allows in noise from the mid-latitude eastward Rossby waves). As for the ER waves, they maintain a relatively important activity (peaks exceeding 150 W^2 m^{-4}) over the eastern and central parts of the domain (Fig. 1.b).

There is a slightly different seasonality between the modes during the spring season. The peak of convective activity related to the MJO occurs in March and April, that of EK waves in April and May whereas the ER is the most active in May (Fig. SM1). The activity of these three modes decreases significantly in June, prior to the onset of the Sahelian phase of the West African monsoon (e.g. Fitzpatrick et al. 2015). This seasonality is further shown by the monthly count of active days of each mode at the reference longitude of 5° E (Fig. 2).

3.2 Synoptic to intraseasonal heatwaves in the Sahel

Previous publications have already elaborated on the statistical characteristics of Sahelian heatwaves at different timescales. There is a general consensus on their short-lasting nature (e.g. Oueslati et al. 2017; Guigma et al. 2020) and their important intensity owing to the hot mean state of the region (red lines in Fig. 2). They are more frequent over the eastern and central Sahel, as shown by the count of springtime heatwave days at each grid-point over the 1980–2017

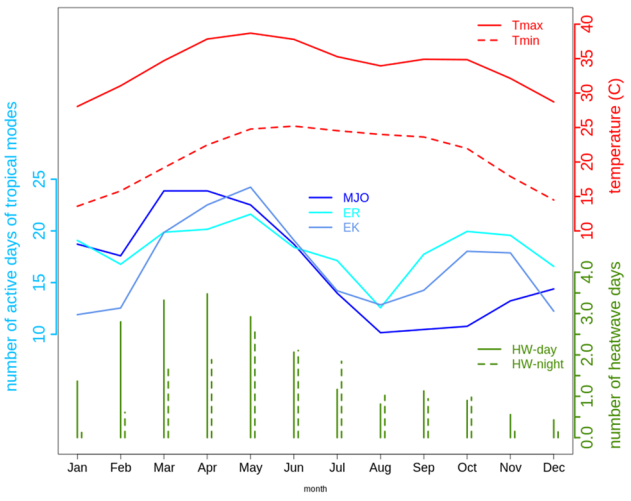

Fig. 2 Seasonality of the activity of tropical modes and heatwave occurrence. Bluish lines :monthly count of active days of the MJO, EK and ER waves as detected at the reference longitude of 5° E between the equator and 10° N (the definition of an active day is given in Sect. 2.3). Green histograms: monthly count of the number of daytime (solid bars) and nighttime (dashed bars) heatwave days spatially averaged over the Sahel domain. Red lines: Monthly values of Tmax (solid lines) and Tmin (dashed lines) spatially averaged over the Sahel domain

period in Fig. SM2 (which provides the sampling basis of heatwaves for this study). As with tropical modes, the frequency of occurrence of synoptic to intraseasonal scale heatwaves has a moderate seasonality. Figure 2 shows that daytime heatwaves are mostly observed between February and June, with a peak in April. On the other hand, nighttime heatwaves occur mainly between March and July with May standing as the most heatwave-prone month. There is thus a shift of nighttime heatwaves with respect to their daytime counterparts. The main reason for this is probably the larger dependence of Tmin (and thus nighttime heatwaves) on low-level moisture whose penetrations into the Sahel are more frequent closer to the onset of the monsoon (Couvreux et al. 2010; Mera et al. 2014).

3.3 Modulation of heatwave probability of occurrence by tropical modes

This section first discusses the impact that each tropical mode, taken separately, has on heatwave occurrence, before analysing the outcome of the superposition of several modes.

3.3.1 Heatwave modulation by modes taken separately

Figure3 shows the phase-longitude diagram of the modulation of heatwave probability (MP) averaged over the Sahel band (10° N–20° N) for the MJO, ER and EK waves during the spring season. Among these three investigated modes, the MJO stands as the lead modulator of heatwave occurrence in the Sahel (Fig. 3a, b) and its eastward propagation is clearly reflected in the modulation MP pattern. Overall, phases 1 to 4 are associated with higher heatwave probability than the climatological probability of occurrence. The values of MP, averaged over the Sahel band, can be as high as 1 (i.e. heatwaves are twice more likely under these phases than according to their climatology). Reversely for phases 5–8, the probability of heatwave occurrence is lower than usual. For these phases, MP is typically below − 0.5, meaning that the probability of occurrence is less than half of its climatological value. The patterns are relatively similar for daytime and nighttime heatwaves, but it is apparent that the stripe of positive MP values is wider in Tmin heatwaves than in Tmax (red stripe in Fig. 3a vs. b), and reversely for the stripe of negative MP values (blue stripe in Fig. 3a vs. b), especially over the western Sahel.

The modulation of Sahelian heatwaves by the ER wave (Fig. 3c, d) is less important than by the MJO. Heatwave probability of occurrence is mostly below normal when the ER wave is in phases 5 to 8 with values of MP generally higher than − 0.5 (i.e. of lower intensity than observed for the MJO). In phases 1 to 4, there is a higher heatwave risk than normal over much of the Sahel, with positive MP values although usually lower than 1. It should be noted that the

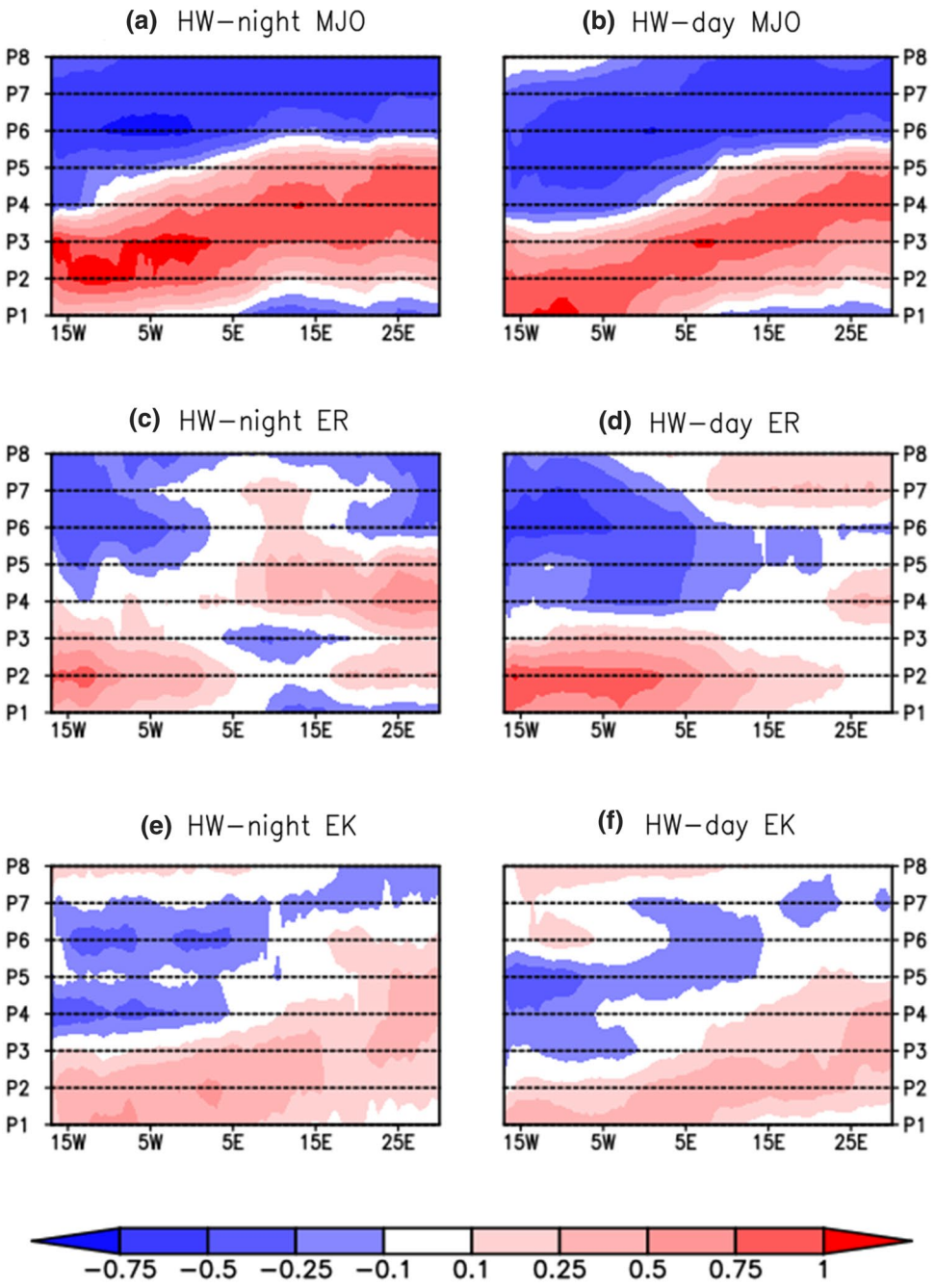

Fig. 3 Phase-longitude diagrams of the modulation of (left panel) nighttime and (right panel) daytime large-scale heatwave probability of occurrence by the MJO, ER and EK waves during MAMJ averaged over the Sahel band (10° N–20° N). The modulation corresponds to the variable MP defined in Sect. 2.4 (Eq. (4)) as a comparison of heatwave probability of occurrence in a given active phase versus the climatological probability. Significance was tested at the probability 0.05 level, using bootstrap resampling of tropical mode active days, with 1000 repetitions

modulation by the ER wave is more sensitive to the diurnal cycle and geographic location than the two other modes. For example, daytime heatwaves over the eastern Sahel are only marginally affected by the activity of the ER wave whereas nighttime heatwaves are much more impacted. On the other hand, over the western Sahel, the modulation is more important for daytime than nighttime heatwaves (this is valid for both positive and negative modulations).

The spatial patterns of the modulation of heatwaves by the EK wave (Fig. 3e, f) are similar to that of the MJO with marked eastward propagation in both cases. However, they present narrower stripes and lower magnitude than with the MJO. The values of MP are indeed in most cases absolutely below 0.5, making the EK wave the least important of the three modes for heatwave occurrence in the Sahel. They present only little sensitivity to the diurnal cycle.

The amplitude of tropical modes, as stated in Sect. 2.3, does not affect the spatial distribution of MP. On the other hand, with increasing amplitudes, the values of MP are slightly increased (without changing their sign). This is illustrated in Fig. SM3, using a minimum amplitude of 2. Therefore, the stronger the amplitude of tropical modes,

the more confident the changes of heatwave probability described above are.

The main reason why the MJO has a greater influence on heatwaves than the ER and EK waves is very likely related to its spectral properties. Heatwaves are slowly varying events whose minimum duration is set to three days here. Therefore, for a given mode to influence their occurrence, it should be able to sustain conditions which are favourable to the heating of the atmosphere for a long-enough amount of time. Evidently, the longer the period of a mode the higher its ability to develop such conditions. This sensitivity of the modulation to the temporal scale corroborates previous results by Schlueter et al. (2019a) who investigated the modulation of precipitation in West Africa by tropical modes. Indeed, they found that, on the scale of three days, the MJO, ER and EK waves have an equal importance on precipitation while on the scale of a week, the effect of EK wave becomes marginal and beyond 20 days, the MJO is the only mode able to significantly contribute to precipitation variability. Besides, the additional constraint on the spatial extension of heatwaves may also favour the MJO. Consequently, the results of this study imply that the smaller the wavenumber of a mode, the more likely this mode can trigger heatwaves as it is also more able to promote warming conditions that spread over large areas.

It should be noted that the patterns of the modulation of heatwaves shown at the seasonal scale are generally consistent across the different months. However, some differences are noticeable, especially with nighttime heatwaves, for some modes. Thus, phases 1 to 4 of the ER wave lead to a decreased probability of nighttime heatwave occurrence over the central Sahel (broadly between 0° E and 20° E) in early spring (March-April) whereas the probability is increased in late spring (May-June), and reversely for phases 5 to 8 (Figs. SM4.a vs. SM4.b). For the EK wave, the decrease of heatwave probability observed in phases 5 to 8 is much more pronounced in late spring than in early spring (Figs. SM4.c vs. SM4.d).

3.3.2 Heatwave modulation by superposition of modes in various phases

Section 3.1 evidenced the need for special consideration of instances where multiple tropical modes are superposed. These superpositions may occur on any phase of the modes. For conciseness purpose, only the most convectively suppressed phase (phase 1) and the most convectively enhanced phase (phase 5) are investigated in the present section. However, it should be noted that, although these phases represent the extremes of the convective activity driven by the modes in the region, they do not necessarily correspond to the peak of their effects on heatwaves as shown in Fig. 3. It is therefore possible to consider other phases when assessing the effect of the superposition of multiple modes on heatwaves.

Sample sizes of different combinations of modes in their phases 1 and 5 are relatively moderate, not exceeding 50 days (Table 3) but allow an insight as to how (much) these configurations impact Sahelian heatwave occurrence. The combinations can be mutually constructive (i.e. all modes on the same phase) or conflicting (e.g. one mode in an enhanced phase and another in a suppressed phase).

Figure4 presents the zonal averages over the Sahel domain (10° N–20° N) of the modulations by pairs of tropical modes. The superposition of the ER wave and the MJO gives relatively similar results for daytime and nighttime, at least over the eastern Sahel (Fig. 4a, b). When these modes co-occur in a constructive way, the resulting MP pattern is comparable to the one obtained when they occur separately and mainly consists in dipolar MP structures: for the suppressed case, an increase of heatwave probability in the western Sahel and a decrease in the eastern Sahel (red dotted lines in Fig. 4a, b), and conversely for the enhanced phase (blue solid lines in Fig. 4a, b). When the MJO and the ER wave are conflictingly superposed, there is a decrease of heatwave probability in most cases (orange dotted lines and green solid lines in Fig. 4a, b). A few exceptions to this include an increase of daytime heatwave probability over the western Sahel when an enhanced ER wave and a suppressed MJO are superposed (orange dotted line in Fig. 4a), and an increase of both daytime and nighttime heatwave probability over the eastern Sahel when the ER wave is in a suppressed phase and the MJO in an enhanced phase (green solid lines in Fig. 4a, b).

The superposition of the EK wave onto the MJO (Fig. 4c, d) leads to modulations of relatively large magnitude which generally take the sign of a singular modulation by the MJO. Similarly to the combined MJO-ER modulation, dipolar patterns are observed as a result of constructive superpositions

Table 3 Counts (in number of days) of co-occurrences of tropical modes in their most suppressed (phase 1) and most enhanced (phase 5) phases by pairs

	MJO		
EK	Phase 1	Phase5	29
	Phase5	44	
	42	49	
	MJO		
ER	Phase 1	Phase5	
	Phase5	54	24
	25	56	
	ER		
EK	Phase 1	Phase5	42
	Phase5	33	
	31	28	

The counts do not exclude the presence of a third mode

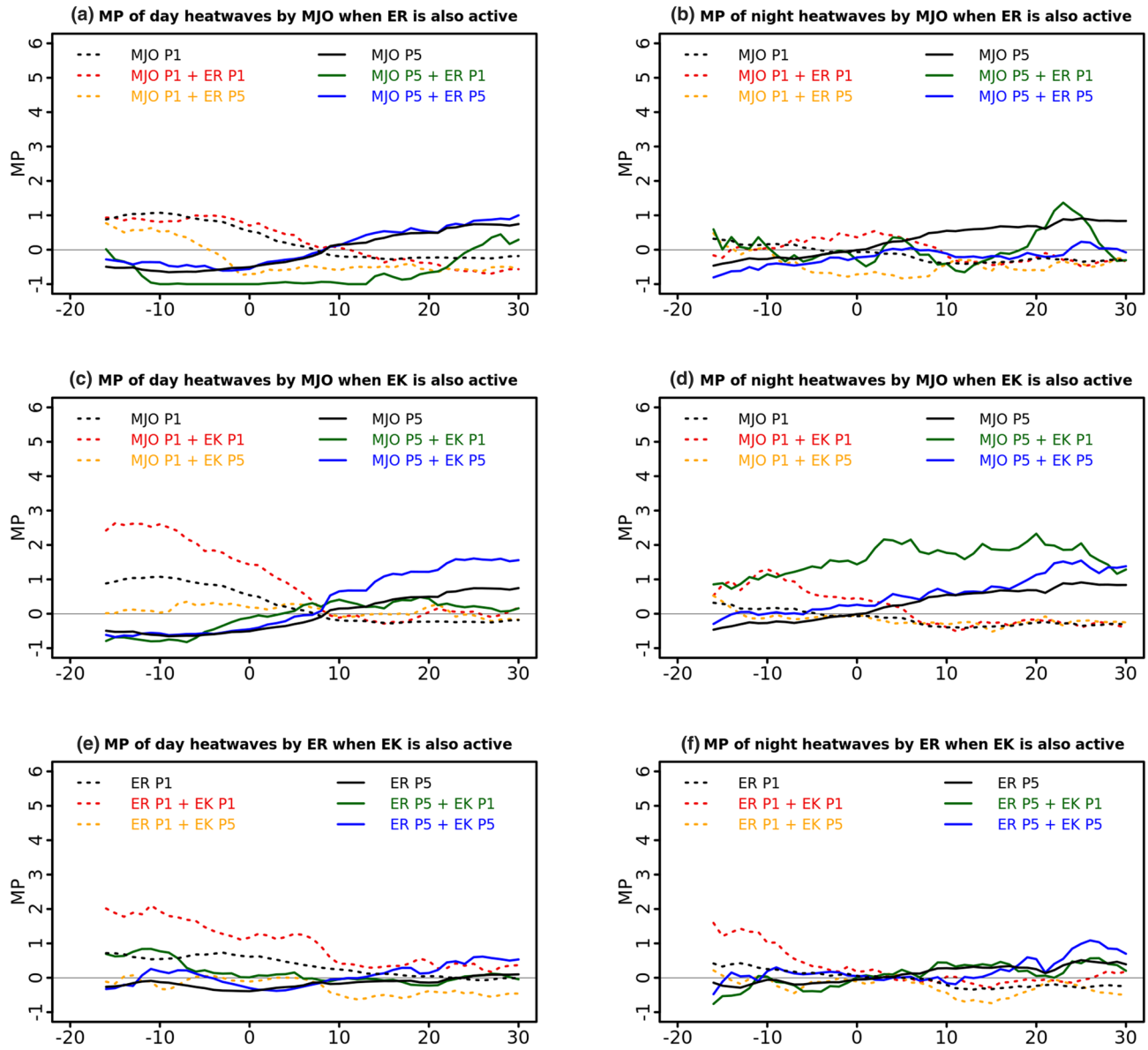

Fig. 4 Zonal averages (10° N–20° N) of the modulation of heatwave probability of occurrence (MP) by superposition of tropical modes during MAMJ. See Sect. 2.4 (Eq. (6)) for details regarding the method. Significance was tested at the 0.05 probability level, using bootstrap resampling of tropical mode active days, with 1000 repetitions

of the MJO and the EK wave. Heatwave probability is increased over the western Sahel (especially at daytime), in opposition to a relatively small decrease over the eastern Sahel when both modes are in their suppressed phases (red dotted lines in Fig. 4c, d). When they are both in their enhanced phases, heatwave occurrence is increased over the eastern Sahel whereas over the western Sahel it is either decreased (case of daytime heatwaves; blue solid lines in Fig. 4c) or unchanged (case of nighttime heatwaves; blue solid lines in Fig. 4d). The conflicting configuration in which the MJO is in phase 1 has only minor impacts on heatwave occurrence in the Sahel (orange dotted lines in Fig 4c, d). On the other hand, in the contingency where the MJO is in phase 5 and the EK wave in phase 1, the modulation of daytime heatwaves is very close to that observed with the MJO alone (green solid lines in Fig. 4c) whilst nighttime heatwave probability is significantly increased throughout the Sahel (MP often exceeds 2; green solid lines in Fig. 4d).

Finally the superposition of the ER and EK waves generally causes only minor changes to Sahelian heatwave probability (Fig. 4e, f). However when both modes are in a suppressed phase, the probability of heatwave occurrence is significantly augmented over the western Sahel (a modulation of up to 2).

In summary, the superposition of multiple modes over the African domain can substantially increase heatwave probability over the western Sahel when they are all in a convectively suppressed phase and over the eastern Sahel when they are all in a convectively enhanced phase, while the outcome for conflicting superpositions depends on the modes under consideration.

3.4 Modulation of heatwave intensity

Heatwave intensity is overall less sensible to tropical modes than the probability of occurrence. Some significant patterns are however obtained with the MJO and ER wave and are shown in Fig. 5. This figure reveals that the intensity of heatwaves is increased when the MJO and the ER waves are in phases 4 to 7, with the modulation MI often reaching 0.4. On the other hand, the intensity is decreased in phases 1 to 3 of the MJO and ER wave, and MI can also get below − 0.4. Finally, the influence of EK waves on

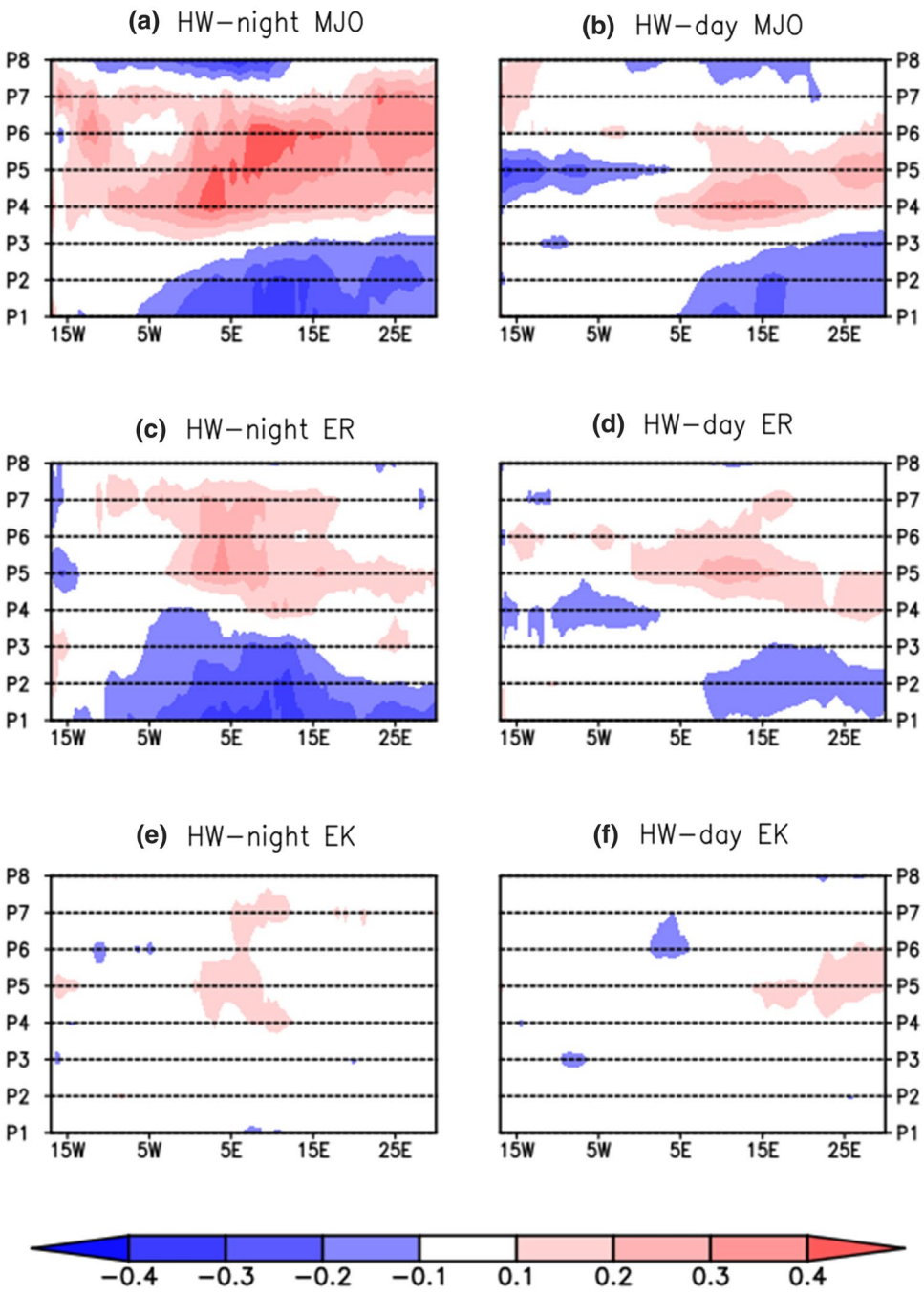

Fig. 5 Phase-longitude diagrams of the modulation of (left panel) nighttime and (right panel) daytime large-scale heatwave intensity by the MJO, ER and EK waves during MAMJ averaged over the Sahel band (10° N–20° N). The modulation corresponds to the variable MI defined in Sect. 2.4 (Eq. (5)) as a comparison of heatwave average intensity in a given active phase versus the climatological intensity of heatwaves. Significance was tested at the 0.05 probability level, using bootstrap resampling of tropical mode active days, with 1000 repetitions

heatwave intensity is quite minor (Fig. 5e, f). Nighttime heatwave intensity is also more affected than daytime heatwave intensity (Fig. 5a, c vs. Fig. 5b, d). From a spatial point of view, the modulation is more marked over central and the eastern Sahel than over the western Sahel.

A comparative examination of the patterns of MP (Fig. 3) versus that of MI (Fig. 5) shows that the two do not match exactly, and this can have implications for heatwave risk management, especially for nighttime heatwaves whose intensity is more impacted by tropical modes. Thus, in phases 6 and 7 of the MJO, nighttime heatwaves are less probable but are more intense (Figs. 3a vs. 5a). Conversely, they are more probable in phases 2 and 3 of the MJO but less intense. When the MJO is in phase 4, it poses a higher risk because heatwaves are both more probable and more intense. This is also the case when the ER wave is in phases 4 to 7 (Figs. 3a vs. 5a).

3.5 Potential mechanisms of modulation

Previous studies (e.g. Oueslati et al. 2017; Guigma et al. 2020) have pointed to the increase of longwave radiation at the surface due to water vapour greenhouse effect and hot air advection as processes underpinning Sahelian heatwaves. This motivates the composite analysis of thermodynamic and dynamical variables presented below for active phases of the modes. The aim here is to provide an insight as to how heatwave processes are impacted by the physical conditions created by tropical modes.

From Fig. 6a it is apparent that the patterns of the advection of heat into the Sahel, although patchy, are relatively consistent with that of the modulation of heatwave occurrence. Increased heatwave occurrence is indeed broadly associated with hotter air advection whereas cooler air advection goes with a decrease of heatwave probability (except over a narrow area around 20° E). The influence

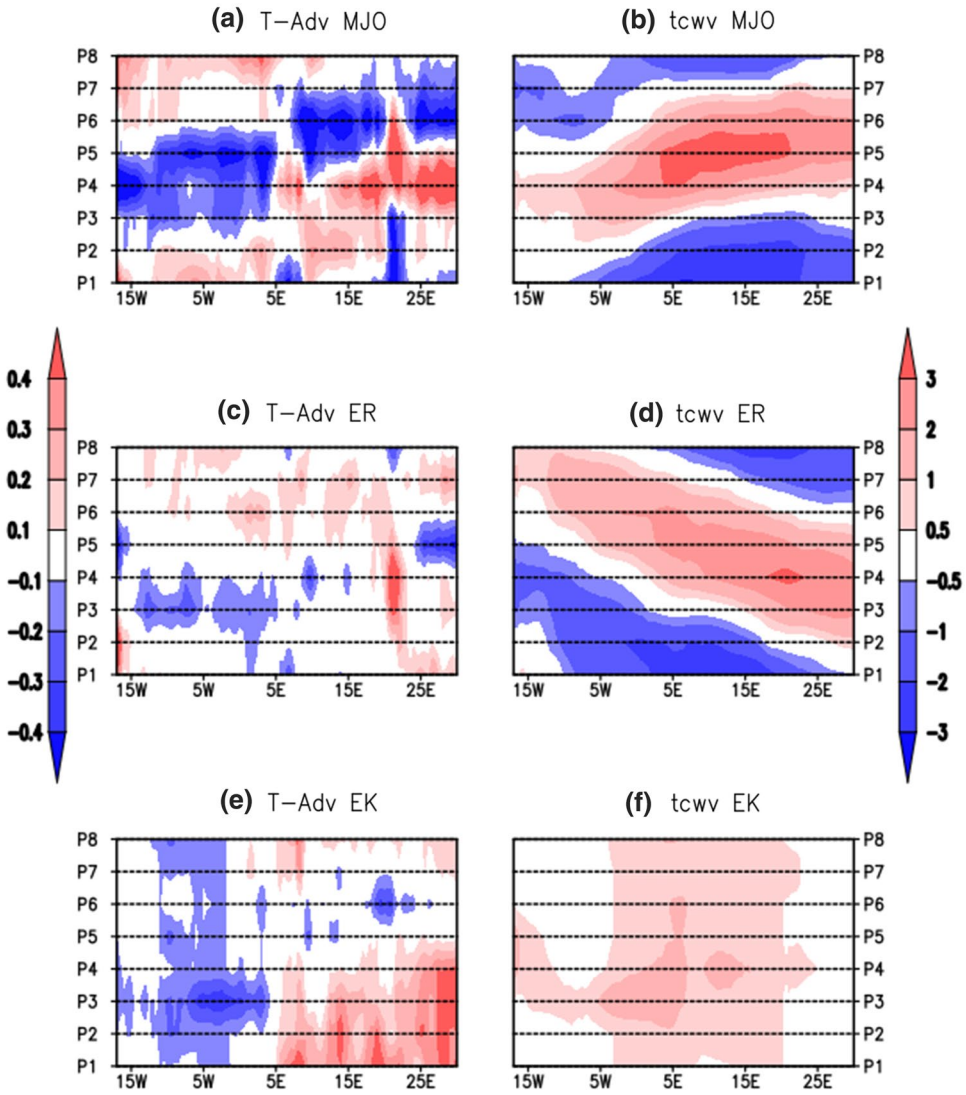

Fig. 6 Phase-longitude diagrams of the composite of daily anomalies of (left panel) heat advection in K day^{-1} and (right panel) precipitable water in mm over active phases of the MJO, ER and EK waves during MAMJ averaged over the Sahel band (10° N–20° N). Significance was tested using a Student t-test at the 0.05 probability level

of tropical modes on heatwave occurrence is also due to their control on water vapour and its associated longwave radiative effect. As shown in Fig. 6, over the eastern Sahel and in phases 4 and 5, the higher probability of heatwave coincides with a positive anomaly of precipitable water reaching 3 mm on zonal average (the longwave radiation and precipitable water patterns are very similar, not shown). However, the MJO-induced precipitable water anomaly has its greatest impact on heatwave intensity. Phases 4 to 7, which are associated with higher heatwave intensity, are also those for which the anomaly of precipitable water is positive; reversely, in phases 1 to 3 where heatwave intensity is lower, there is a dry anomaly especially marked over the eastern Sahel (Figs. 5a, b vs. 6b). The stronger dependence of nighttime heatwaves on water vapour (Guigma et al. 2020; Largeron et al. 2020) likely explains why their intensity is more affected by the MJO (Fig. 5a vs. b).

Associated with ER wave, an advection of hot air is present too, though mostly confined to the eastern Sahel (Fig. 6c) which could be linked to the increase of heatwave probability in phases 3 to 5 for nighttime heatwaves, and 7 to 8 for daytime heatwaves (Fig. 3c, d). Atmospheric water vapour itself is not directly linked to heatwave probability but its anomalies give an insight into other processes. Over the western Sahel, the increase of heatwave probability in phases 1 to 3 (Fig. 3c, d) can be connected to the negative anomaly of precipitable water (Fig. 6d), which is associated with reduced cloudiness and increased incoming solar radiation (not shown) which is a frequent underlying process of Sahelian heatwaves (Guigma et al. 2020). The reverse interpretation can be made for phases 5 to 8, where increased cloudiness and precipitable water (Fig. 6d) weaken incoming solar radiation (not shown) and are associated with a decrease of heatwave probability (Fig. 3c, d). As with the MJO, water vapour has a direct impact on heatwave intensity. The patterns of precipitable water (Fig. 6d) and of the modulation of heatwave intensity (Fig. 5c, d) are indeed relatively close.

The links between the EK wave-modulated patterns of heatwave occurrence and physical processes are less evident given that the anomalies of the EK wave are predominantly confined to the equatorial region as per theory (not shown). Nonetheless, it is apparent that advection of hot air (which is important in magnitude) in phases 1 to 5 plays an important role especially over the eastern Sahel (Fig. 6e), where heatwave probability is increased. On the other hand, advection of cooler air over the western Sahel in phases 4 to 7 may also explain the decrease of heatwave probability there.

While phase-longitude diagrams are efficient at summarising the physical conditions promoted by tropical modes in their different phases, they do not inform on their full horizontal distribution. To get around this issue, Fig. 7 shows for illustration purposes, the maps of these variables composited over the most convectively suppressed and enhanced phases (phases 1 and 5 respectively) of the MJO. They are superimposed with low-level (925 hPa) wind anomalies in order to assess the origins of the heat (whose climatological distribution is depicted in Lavaysse et al. 2009). The suppressed phase of the MJO is associated with a low level northeasterly wind anomaly across the Sahel (which is part of an anticyclonic cell) carrying the drier and hotter air from the Sahara desert and the eastern Sahel towards the western Sahel (Fig. 7a, c). As a result, in the western part of the Sahel, advection of hotter air (with magnitude reaching 1.5 K day^{-1}), leads to an increase of heatwave probability (Fig. 3a, b). On the other hand the arrival of air masses from higher latitudes causes drying and cooling over the eastern Sahel, reducing longwave radiation, hence the decline of heatwave probability in this region (Fig. 3a, b). Reversely, when the MJO is convectively enhanced, the low-level flow presents a cyclonic anomaly characterised by a northwesterly wind anomaly over the western Sahel/Sahara, which advects cooler air (Fig. 7d) leading to a decrease of heatwave probability (Fig. 3a, b). Over the eastern Sahel/Sahara, a southwesterly wind anomaly carries humid air from the equatorial region (Fig. 7b), causing an increase of heatwave probability (Fig. 3a, b) associated with increased longwave radiation.

These results agree with previous findings by Moron et al. (2018a) who also showed the importance of the modulation of low-level circulation by the MJO in increasing/decreasing temperature over tropical Africa. They also extend them further by documenting the associated physical processes.

4 Case-study of the April 2003 heatwave

4.1 Motivation and description of the heatwave

Guigma et al. (2020) showed that intraseasonal heatwaves over the Sahel are generally short-lived (average duration not exceeding five days), with only a small portion of them (about 10%) occurring concurrently at daytime and nighttime. Yet, in terms of impacts on health, longer lasting daytime events which persist during the nighttime are expected to be the most harmful (Schär 2016; Murage et al. 2017). Given their small sample size, the findings of the broad statistical analysis of heatwave modulation by tropical modes (Sect. 3) may not be directly applicable to them, especially since daytime and nighttime were dissociated. From this perspective, it is relevant to investigate them through a representative case study as also suggested by Guigma et al. (2020). This is the reason why the Sahelian heatwave which took place during the first half of April 2003 was selected. It is characterised by (i) a relatively long duration (more than 10 days) and (ii) a simultaneousness of daytime and

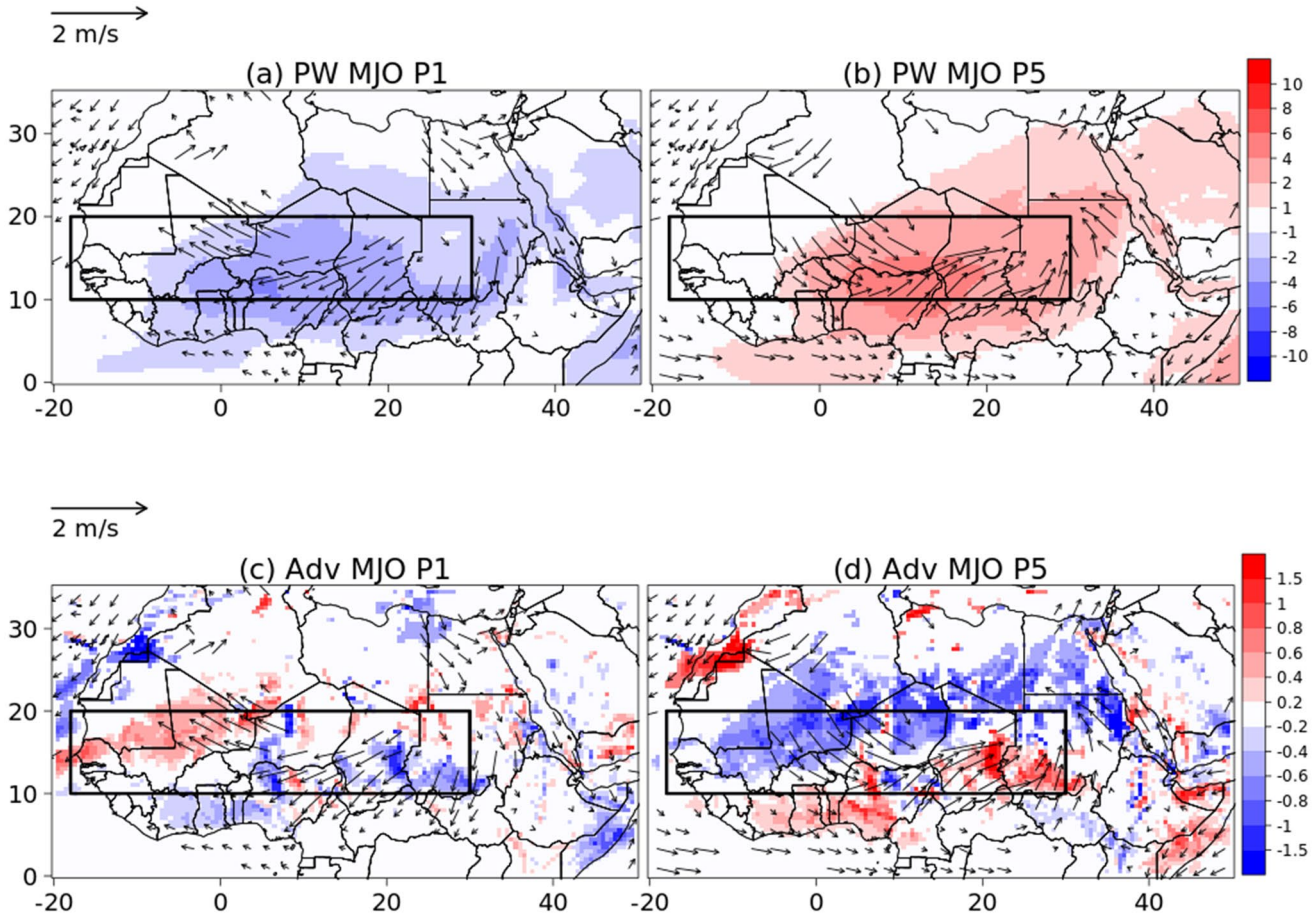

Fig. 7 Composite of daily anomalies of **a**, **b** precipitable water in mm and **c** **d** 925 hPa heat advection in K day^{-1} over phases 1 and 5 of the MJO. Superimposed vectors are anomalies of horizontal wind at the 925 hPa level. Significance was tested using a Student*t* test at the 0.05 probability level. The rectangular box delimits the Sahel region

nighttime heatwaves over a common wide domain. This event is also mentioned as a severe one in Oueslati et al. (2017) but, to the best of the authors' knowledge, it has never been investigated. The daytime heatwave started first, on 03 April, while the nighttime one started on 04 April, and they both ceased on 15 April. From a spatial point of view, the time-longitude diagram of temperature anomalies averaged over the Sahel band of 10° N–20° N (Fig. 8a) reveals that the heatwave kicked off over the eastern Sahel (in northern Chad/Sudan more precisely; not shown), stood there until approximately 08 April, moved towards the central Sahel before heading back to the east on its latest days. April 2003 was also marked by an important intraseasonal variability of temperature, as revealed by a wavelet decomposition of Tmin and Tmax (not shown). The variability of temperature at these scales is particularly relevant here as it suggests an important modulation by the high-frequency modes of climate variability, including the MJO and equatorial waves. Finally in April 2003, there was no incursion of extratropical perturbations into West Africa, nor any strong interannual temperature anomaly (not shown), therefore allowing to get a "pure" modulation by tropical modes.

4.2 Activity of tropical modes in April 2003

Figure8b shows a time-longitude diagram of highpass-filtered OLR anomalies averaged over the Guinean band to which the mode-filtered OLR anomalies (averaged over the same latitudinal band) are superimposed as contours. This is a common technique used in tropical mode investigations (e.g. Schreck and Molinari2011; Ventrice and Thorncroft2012; Lafore et al. 2017).

Over the heatwave period (i.e. first half of April), two MJO packets crossed West Africa (black contours in Fig. 8b). For the first packet, it is its convectively suppressed phase which is relevant to the heatwave. It penetrated West Africa during the second half of March 2003 and reached the Indian Ocean near 10 April. As for the second packet, its convectively enhanced phase (which is the one relevant to the heatwave) entered West Africa in early April, reached

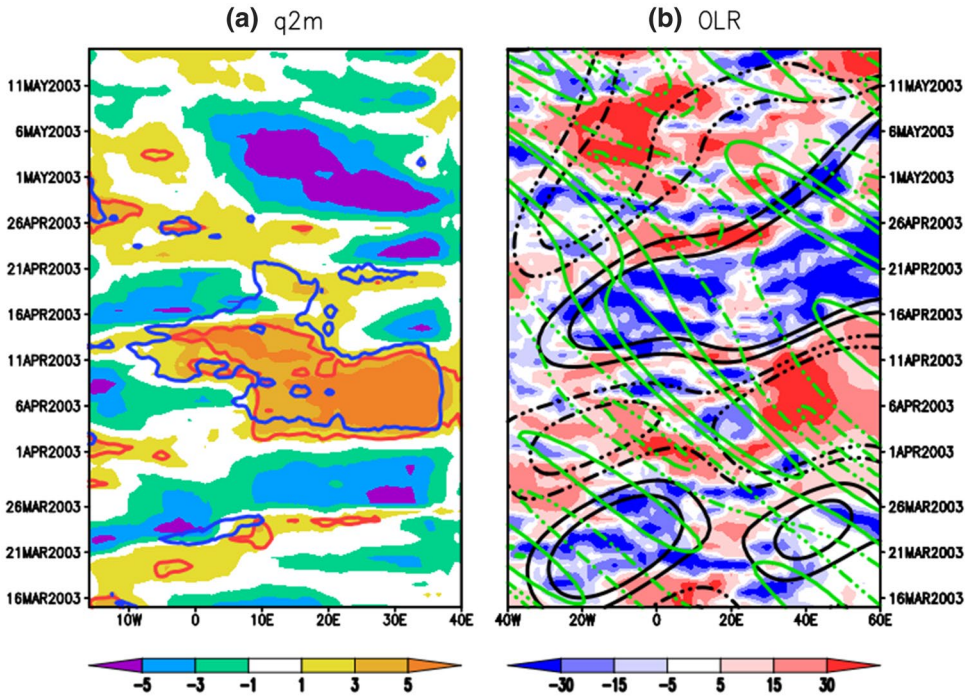

Fig. 8 Time-longitude diagrams of 90-day highpass filtered anomalies of **a** 2 m specific humidity (shades; units in g Kg^{-1}), daily minimum (blue contours) and maximum (red contours) temperature averaged over the 10°–20° N band and **b** OLR (shades; units in Wm-2) superimposed with MJO (black contours) and ER (green contours) wave-filtered OLR anomalies averaged over the 0–10° N band between 15 March and 15 May 2003. In **a** the contour level is 2K for both the minimum and the maximum temperature. In **b**, the contour levels for the MJO and ER-wave filtered anomalies are 5 and 10 W m^{-2} (–5 and − 10 W m^{-2}) for the solid (dashed) lines

its maximum amplitude over Central West Africa (10°–10° E) in mid-April before exiting the African domain after weakening at its eastern parts. An ER wave packet (green contours in Fig. 8b) also travelled westwards across West Africa during the first half of April 2003. The enhanced phase was the first to reach Africa from the eastern coast and was observed over Sahelian longitudes in early April. It eventually strengthened in mid-April, when it met with the enhanced phase of the second MJO packet. The suppressed phase reached West Africa after 15 April.

4.3 Overall physical processes during the event

An analysis of the thermodynamic budget emphasizes that two processes, namely longwave heating (Fig. 9a) and hot air advection (Fig. 9c) largely shaped the April 2003 heatwave. Indeed, during this period, the area covering Chad and Sudan is home to a strong hot air advection, reaching 1.5 K day^{-1} at some places. As a result, the thermal gradient between the atmosphere and the ground is weakened, leading also to a decrease of the sensible heat flux according to ERA5 (not shown). As for the net longwave heating, it is observed over the western and central Sahel/Sahara, and most importantly over the southeasternmost parts of the Sahel with a maximum exceeding 20 Wm^{-2}. This longwave anomaly results mostly from a greenhouse effect (GHE) of water vapour, as testified by the pattern of precipitable water which presents a similar anomaly (Fig. 9b). Dust aerosol (an important constituent of the Sahelian atmosphere) was not significant in April 2003 according to MODIS data (not shown), precluding any significant contribution from this component to the observed warming.

The longwave warming anomaly at the surface is also a footprint of a reinforcement of convective activity over West Africa. Besides the positive anomaly of precipitable water, there is indeed a low-level cyclonic anomaly with monsoonal wind surges into the Sahel, advecting water vapour from the Gulf of Guinea (Fig. 9d). Furthermore, the patterns of low-level circulation, hot air advection and precipitable water observed during the heatwave period are very similar to their composite mean anomalies over the convectively enhanced phases of the MJO (Fig. 7b, d). As a reminder, heatwave probability is increased over the eastern Sahel when the MJO is in these phases (Fig. 3a, b). As such, the April 2003 event, despite being exceptional (by its length and daytime/nighttime concomitance), adheres to the general findings presented in Sect. 3, both in terms of the physical conditions created by tropical modes and the outcome for heatwave occurrence. The next section emphasises this in more detail.

4.4 Day to day evolution of the heating processes and impact of tropical modes

A day to day analysis of the heatwave event further allows a deeper insight into the evolution of different processes shaping the heatwave and the role played by tropical modes.

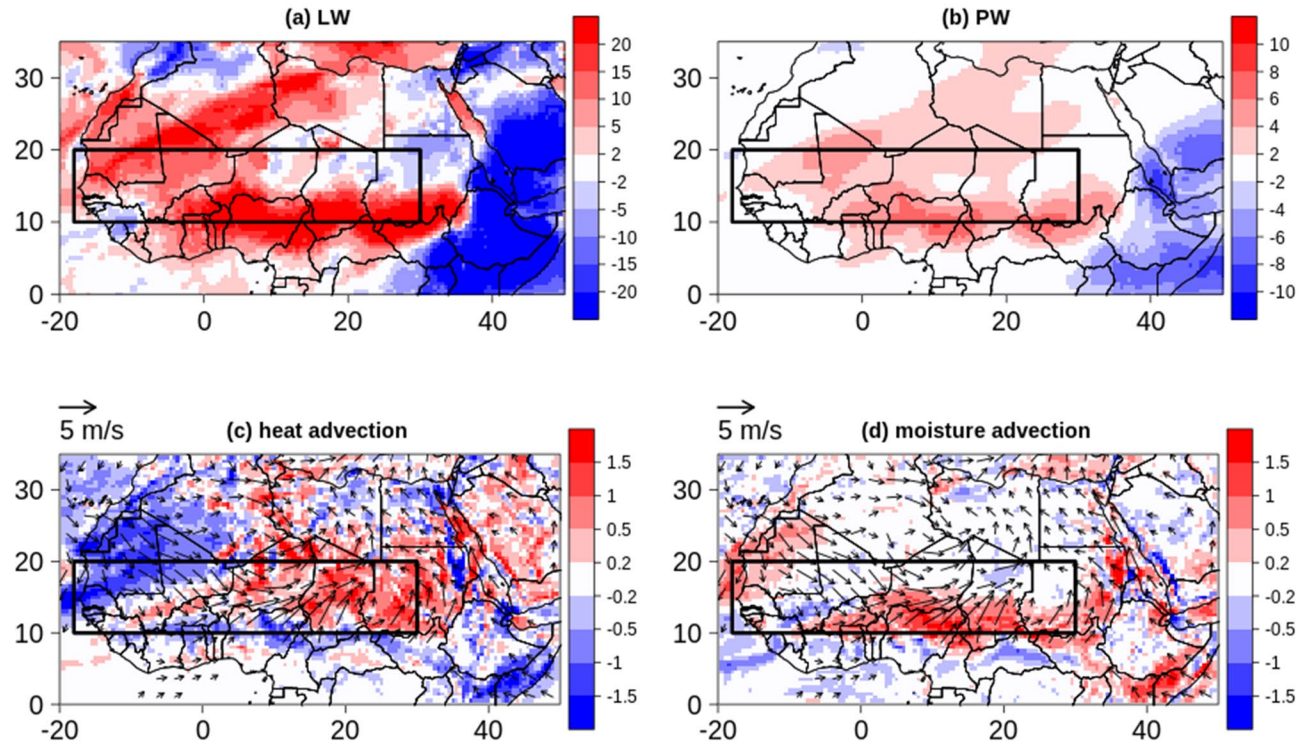

Fig. 9 Anomalies of **a** Net longwave radiation at the surface in Wm^{-2}, **b** Precipitable water in mm, **c** 925 hPa level heat advection in K day^{-1}, **d** 925 hPa level specific humidity advection (g kg^{-1} day^{-1}) averaged over the first half of April 2003. Vectors in **c** and**d** represent the 925 hPa level wind anomalies (only magnitudes greater than 1 m s^{-1} are shown). All quantities are obtained from ERA5. The rectangular box delimits the Sahel region

4.4.1 An initial role of heat advection fostered by the MJO (late March – 04 April)

Figure10a shows that the onset of the heatwave over the eastern Sahel was preceded by a sustained advection of hot air in late March and during the first days of April. The low-level wind pattern in Fig. 9c shows that the hot air originated from the central and southern Sahel (approximately 10° N–13° N), where the West African Heat Low (WAHL) is typically located at this time of the year (Lavaysse et al. 2009). The projection of the activity of the different modes on this process (described in Sect. 2.4) shows that the MJO (which was in a convectively suppressed phase at that time; Fig. 8b) was its main driver. In Fig. 10a, the MJO-regressed anomalies (black contours) indeed encapsulate the heat advection. Therefore the MJO acted in suppressing convection over the WAHL area, causing a warming which is further advected to the northeastern Sahel and led to the heatwave initiation.

4.4.2 A progressive takeover by water vapour GHE led by the ER wave (05–08 April)

Despite a progressive decrease of heat advection after the onset, the heatwave was sustained mainly as a result of the arrival of moist air in the Sahel from the subequatorial region (Fig. 9d), causing a water vapour GHE as illustrated in Fig. 10b (using observed incoming longwave radiation at the surface, a proxy for GHE). In-situ observations at the Demokeya station (30.5° E; 13.3° N) also confirm the progressive increase of water vapour during this stage of the heatwave (Fig. SM5). The regressed values of incoming longwave radiation (green contours in Fig. 10b) as well as of precipitable water (green contours in Fig. 10c) on the ER wave are positive and match relatively well the spatial structure of the anomalies of these variables, suggesting a preponderant role of this wave at this stage of the event. Thus, agreeingly with its expected impact on heatwaves discussed in early spring (Sect. 3), the convectively enhanced ER wave organised a low-level meridional transport of water vapour into the eastern Sahel, and, through longwave radiation, heated up the region. The statistical findings are further strengthened since consistency is shown here across different observational (satellite) datasets.

4.4.3 Final stage: a reinforcement of the GHE forced by the MJO (09–14 April)

The westward motion of the ER wave allowed the heating to reach the central and western parts of the Sahel. From 09

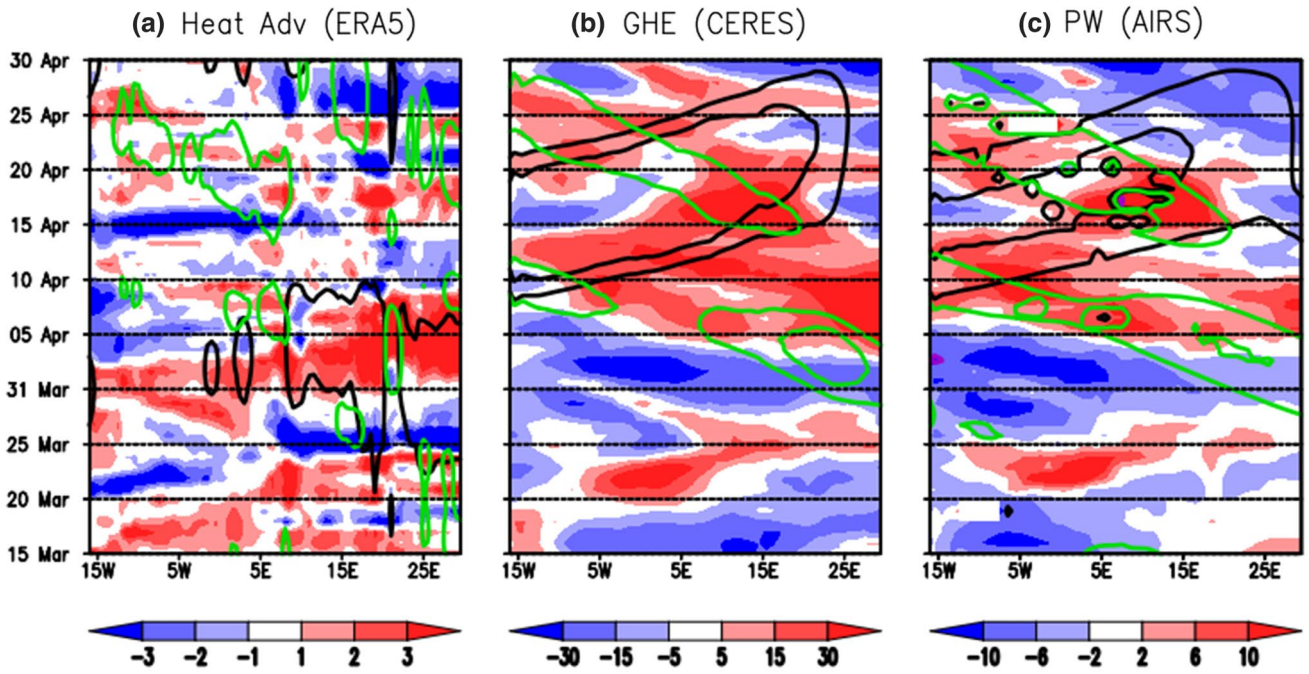

Fig. 10 Time-longitude diagram of **a** ERA5 heat advection at the 925 hPa level. Shades represent the daily highpass filtered anomalies and contours the regression of these anomalies on the MJO (black contours) and ER waves (green contours). Units are in K day^{-1} and the contour level is 0.1 (negative levels are omitted). **b** CERES incoming longwave radiation. Shades represent the daily highpass filtered anomalies and contours the regression of these anomalies on the MJO (black contours), the ER waves (green contours). Units are in W m^{-2} and the contour levels are 2.5 and 5 (negative levels are omitted). **c** AIRS precipitable water. Shades represent the daily highpass filtered anomalies and contours the regression of these anomalies on the MJO (black contours) and ER waves (green contours). Units are in mm and the contour levels are 1 and 3 (negative levels are omitted). All the quantities are averaged over the 10° N–20° N latitudinal band between 15 March and 30 April 2003

April, the convectively enhanced phase of the second MJO packet entered the West Africa sector (Sect. 4.2, Fig. 8b). It further increased moisture through a zonal transport of water vapour from the Atlantic into the Sahel. As a result, the GHE effect reached its peak (above 30 Wm^{-2}) leading to an intensification of temperature anomalies, especially at night (Fig. 8a). The leading role of the MJO on this stage of the heatwave is discernible from the regression of the relevant processes on its timeseries (black contours in Fig. 10b, c). Its eastward propagation also dragged the region of maximum heating back towards the eastern Sahel. Again this is predicted by the statistical analysis as it is shown that, through water vapour GHE (Figs. 6b, 7b), convectively enhanced phases of the MJO heat up the eastern Sahel, augmenting heatwave probability therein (Fig. 3a, b). From approximately 15 April, the MJO-driven intensified convection caused organised rainfall events that watered large parts of the heatwave region (Fig. SM6) and led to a decrease of temperature. This eventually ended the heatwave.

It should be noted that the evolution of GHE and precipitable water depicted by ERA5 is very similar to that of CERES and AIRS respectively. Furthermore, the influence of the modes on the evolution of the physical processes is also well captured by ERA5. This is shown by the daily evolution of the regressed fields of interest spatially averaged over grid-cells where the heatwave is detected (Fig. SM7).

In summary, the April 2003 heatwave, from a large-scale point of view, was initiated by a convectively suppressed MJO that promoted hot air advection, and sustained through GHE of water vapour brought in, first by a convectively enhanced ER wave and later on by a convectively enhanced MJO. In addition to supporting the statistical characteristics of heatwave occurrence in the eastern Sahel, this case study also provided an insight on the organisation of the water vapour low-level flow by tropical modes which is an important driver of heatwaves. Thus, it appears that the MJO exerts its control mainly through zonal transport of water vapour whereas the ER wave mostly affects meridional transport.

5 Conclusion and perspectives

Extreme heat represents a growing threat for Sahelian populations, with the latest research stressing that by the end of the century, climate change would make the region reach worrying levels of thermal discomfort (Xu et al. 2020;

Raymond et al. 2020). Therefore, undertaking actions which could mitigate this important issue is a top priority. This study contributes towards this through an analysis of the relationship between tropical modes and Sahelian heatwave events with the view of improving scientific understanding of these extremes. More precisely, it demonstrates that the MJO, ER and EK waves are important factors for the occurrence and - to a lesser extent - intensity of heatwaves in the region during the spring season. Their influence on heatwave occurrence is a function of their convective phase (enhanced or suppressed) and amplitude; it is also distinct for nighttime and daytime heatwaves and varies with the geographical location. Generally, in their convectively suppressed phases, they advect hot air from the climatological location of the WAHL towards the western coast of the Sahel, increasing heatwave probability there. When they are in convectively enhanced phases, they increase longwave warming especially over the eastern Sahel by bringing in water vapour from the Guinean region of Africa. Several tropical modes often overlap over the region. In these situations, heatwaves are more likely to occur over the western Sahel when all modes are in a convectively suppressed phase, and over the eastern Sahel when they are convectively suppressed. The statistical findings were further illustrated by the detailed analysis of a strong Sahelian heatwave event which occurred in April 2003. Hot air advection and longwave radiation, driven by the MJO and ER waves were responsible for a relatively long lasting event that had the particularity of affecting both daytime and nighttime.

From an operational point of view, the heatwaves-tropical modes relationship is important since the wave activity can be used by forecasters as an additional relevant tool to prepare warnings. Moreover, there is a potential for further work aiming at building statistical models of heatwave predictability based on the activity of tropical modes and the interaction between them. The modulation patterns at 5° E shown in the present study can already be used to forecast the likelihood of heatwave occurrence at a given location in the Sahel, taking into account the spectral properties (wavenumber and period) of the modes. For example, when a convectively suppressed ER wave is detected at 30° E, a forecaster in Senegal can expect hot conditions over his/her region in the following 10 days. Better forecast recipes can be obtained from the monitoring of tropical mode activity by reassessing their impact when they are located at longitudes closer to the areas covered by the forecaster, but also at selected longitudes further away (because, given their wavenumbers, tropical modes can impact regions fairly remote from their central position). This therefore calls for more regional coordination between national meteorological services.

Besides, with the amelioration of weather observation networks, the increase of computational capacity and improvement of numerical models, tropical modes are now better represented and predicted (Dias et al. 2018; Janiga et al. 2018; Kim et al. 2018; Bengtsson et al. 2019). These skills can therefore be transferred to heatwave prediction at the intraseasonal scale and thus help to win time for preparedness actions. The authors are already engaged in research in that direction.

Other large-scale drivers of Sahelian heatwaves have been suggested by previous studies (Fontaine et al. 2013; Moron et al. 2018; Guigma et al. 2020). In particular, intrusions of extratropical Rossby waves often combined with tropical plumes can lead to significant increases of temperature and moisture in the Sahel as was the case in April 2010 (Largeron et al. 2020). It is therefore important that future studies also focus on the links between these large-scale features and heatwaves and on the interactions between them and tropical modes.

Finally, it may be important to assess whether the upward trend of Sahelian temperature and heatwave frequency and intensity over the recent past (Fontaine et al. 2013; Moron et al. 2016; Guichard et al. 2017; Ceccherini et al. 2017) is partly attributable to the global warming-induced increased activity of tropical modes over the same period (Song and Seo2016; Adames et al. 2017). This has implications for future projections, as the accuracy of the simulation and future evolution of springtime convection over the Guinean region by climate models might have repercussions on Sahelian heatwave predictions.

Acknowledgements Douglas J. Parker and four anonymous reviewers provided comments that substantially improved the manuscript. This research was supported through the (i) UK NERC/ESRC/DfID Science for Humanitarian Emergencies and Resilience (SHEAR) consortium project 'Towards Forecast-based Preparedness Action' (ForPAc,www.forpac.org), grant NE/P000673/1 and (ii) Future Climate for Africa (FCFA) regional consortium project 'AMMA-2050', grant NE/M02024X/1. KHG was supported by the Peter Carpenter Scholarship for African Climate Science at the University of Sussex, UK. The authors thank Jessica Barbier for assistance with the detection of large-scale heatwaves.

Data availability statement All data used in this study are freely available at the following repositories: ERA5: https://cds.climate.copernicus.eu/cdsapp#!/home. CERES: https://ceres.larc.nasa.gov/data/. AIRS: https://airs.jpl.nasa.gov/data/get-data/standard-data/. Demokeya observed data: http://downloads.hindawi.com/archive/2013/297973.item.1.xlsx and http://downloads.hindawi.com/archive/2013/297973.item.2.xlsx.

References

AIRS Science Team/Joao Teixeira (2013), AIRS/Aqua L3 Daily Standard Physical Retrieval (AIRS-only) 1 degree × 1 degree V006, Greenbelt, MD, USA, Goddard Earth Sciences Data and Information Services Center (GES DISC). https://doi.org/10.5067/Aqua/AIRS/DATA303

Adames ÁF, Kim D, Sobel AH, Genio AD, Wu J (2017) Characterization of moist processes associated with changes in the propagation of the MJO with increasing CO2. J Adv Model Earth Syst 9:2946–2967. https://doi.org/10.1002/2017MS001040

Ardö J (2013) A 10-year dataset of basic meteorology and soil properties in Central Sudan. Dataset Pap Geosci https://doi.org/10.7167/2013/297973

Arkin PA, Ardanuy PE (1989) Estimatingclimatic-scale precipitation from space: a review. J Clim 2:1229–1238.https://doi.org/10.1175/1520-0442(1989)002<1229:ECSPFS>2.0.CO;2

Barbier J, Guichard F, Bouniol D, Couvreux F, Roehrig R (2018) Detection of intraseasonal large-scale heat waves: characteristics and historical trends during the Sahelian spring. J Clim 31:61–80. https://doi.org/10.1175/JCLI-D-17-0244.1

Bengtsson L, Dias J, Gehne M et al (2019) Convectively coupled equatorial wave simulations using the ECMWF IFS and the NOAA GFS cumulus convection schemes in the NOAA GFS model. Mon Weather Rev 147:4005–4025. https://doi.org/10.1175/MWR-D-19-0195.1

Berhane F, Zaitchik B, Badr HS (2015) The Madden–Julian Oscillation's influence on spring rainy season precipitation over equatorial West Africa. J Clim 28:8653–8672. https://doi.org/10.1175/JCLI-D-14-00510.1

Ceccherini G, Russo S, Ameztoy I, Marchese AF, Carmona-Moreno C (2017) Heat waves in Africa 1981–2015, observations and reanalysis. Nat Hazards Earth Syst Sci 17:115–125. https://doi.org/10.5194/nhess-17-115-2017

Cerne SB, Vera CS (2011) Influence of the intraseasonal variability on heat waves in subtropical South America. Clim Dyn 36:2265–2277. https://doi.org/10.1007/s00382-010-0812-4

Couvreux F, Guichard F, Bock O, Campistron B, Lafore J-P, Redelsperger J-L (2010) Synoptic variability of the monsoon flux over West Africa prior to the onset. Q J R Meteorol Soc 136:159–173. https://doi.org/10.1002/qj.473

Davidson O, Halsnæs K, Huq S, Kok M, Metz B, Sokona Y, Verhagen J (2003) The development and climate nexus: the case of sub-Saharan Africa. Clim Policy 3:S97–S113. https://doi.org/10.1016/j.clipol.2003.10.007

Dias J, Gehne M, Kiladis GN et al (2018) Equatorial waves and the skill of NCEP and ECMWF numerical weather prediction systems. Mon Weather Rev 146:1763–1784. https://doi.org/10.1175/MWR-D-17-0362.1

Doelling DR et al (2013) Geostationary enhanced temporal interpolation for CERES flux products. J Atmos Ocean Technol 30:1072–1090. https://doi.org/10.1175/JTECH-D-12-00136.1

Doelling CO, Haney BR, Scarino A, Gopalan, Bhatt R (2016) Improvements to the geostationary visible imager ray-matching calibration algorithm for CERES edition 4. J Atmos Ocean Technol 33:2679–2698. https://doi.org/10.1175/JTECH-D-16-0113.1

Dosio A (2017) Projection of temperature and heat waves for Africa with an ensemble of CORDEX regional climate models. Clim Dyn 49:493–519. https://doi.org/10.1007/s00382-016-3355-5

Duchon CE (1979) Lanczos filtering in one and two dimensions. J Appl Meteor 18:1016–1022. https://doi.org/10.1175/1520-0450(1979)018<1016:LFIOAT>2.0.CO;2

Déqué M, Calmanti S, Christensen OB et al (2017) A multi-model climate response over tropical Africa at + 2 °C. Clim Serv 7:87–95. https://doi.org/10.1016/j.cliser.2016.06.002

Fitzpatrick RGJ, Bain CL, Knippertz P, Marsham JH, Parker DJ (2015) The West African monsoon onset: a concise comparison of definitions. J Clim 28:8673–8694. https://doi.org/10.1175/JCLI-D-15-0265.1

Fontaine B, Janicot S, Monerie P-A (2013) Recent changes in air temperature, heat waves occurrences, and atmospheric circulation in Northern Africa. J Geophys Res Atmos 118:8536–8552. https://doi.org/10.1002/jgrd.50667

Guichard F, Kergoat L, Mougin E, Timouk F, Baup F, Hiernaux P, Lavenu F (2009) Surface thermodynamics and radiative budget in the Sahelian Gourma : seasonal and diurnal cycles. J Hydrol 375:161–177. https://doi.org/10.1016/j.jhydrol.2008.09.007

Guichard F, Kergoat L, Hourdin F, Léauthaud C, Barbier J, Mougin E, Diarra B (2017) Climate warming observed in the Sahel since 1950, In 'Rural societies in the face of climatic and environmental changes in West Africa'. pp 23–42. Sultan B, Lalou R, Sanni MA, Oumarou A (eds), M. A. Soumaré. AN13: 9782709924245 and 978270992426 9$4

Guigma KH, Todd M, Wang Y (2020) Characteristics and thermodynamics of Sahelian Heatwaves analysed using various thermal indices, submitted to Climate Dynamics

Gu G (2009) Intraseasonal variability in the equatorial Atlantic-West Africa during March–June. Clim Dyn 32:457–471. https://doi.org/10.1007/s00382-008-0428-0

Harrington LJ, Otto FEL, Cowan T, Hegerl GC (2019) Circulation analogues and uncertainty in the time-evolution of extreme event probabilities: evidence from the 1947 Central European heatwave. Clim Dyn 53:2229–2247. https://doi.org/10.1007/s00382-019-04820-2

Hersbach H, Bell B, Berrisford P et al (2020) The ERA5 global reanalysis. Q J R Meteorol Soc 146:1999–2049. https://doi.org/10.1002/qj.3803

Hsu P-C, Lee J-Y, Ha K-J, Tsou C-H (2017) Influences of boreal summer intraseasonal oscillation on heat waves in monsoon Asia. J Clim 30:7191–7211. https://doi.org/10.1175/JCLI-D-16-0505.1

Hsu Y, Qian Y, Liu H, Murakami, Gao Y (2020) Role of abnormally enhanced MJO over the Western Pacific in the formation and subseasonal predictability of the record-breaking Northeast Asian heatwave in the summer of 2018. J Clim 33:3333–3349. https://doi.org/10.1175/JCLI-D-19-0337.1

Janiga MA, Schreck CJ, Ridout JA, Flatau M, Barton NP, Metzger EJ, Reynolds CA (2018) Subseasonal forecasts of convectively coupled equatorial waves and the MJO: activity and predictive skill. Mon Weather Rev 146:2337–2360. https://doi.org/10.1175/MWR-D-17-0261.1

Judt F (2020) Atmospheric predictability of the tropics, middle latitudes, and polar regions explored through global storm-resolving simulations. J Atmos Sci 77:257–276. https://doi.org/10.1175/JAS-D-19-0116.1

Kalapureddy MCR, Lothon M, Campistron B, Lohou F, Saïd F (2010) Wind profiler analysis of the African Easterly Jet in relation with the boundary layer and the Saharan heat-low. Q J R Meteorol Soc 136:77–91. https://doi.org/10.1002/qj.494

Kamsu-Tamo PH, Janicot S, Monkam D, Lenouo A (2014) Convection activity over the Guinean coast and Central Africa during northern spring from synoptic to intra-seasonal timescales. Clim Dyn 43:3377–3401. https://doi.org/10.1007/s00382-014-2111-y

Kiladis GN, Straub KH, Haertel PT (2005) Zonal and vertical structure of the Madden–Julian oscillation. J Atmos Sci 62:2790–2809. https://doi.org/10.1175/JAS3520.1

Kiladis GN, Thorncroft CD, Hall NMJ (2006) Three-dimensional structure and dynamics of African Easterly waves. Part I: observations. J Atmos Sci 63:2212–2230. https://doi.org/10.1175/JAS3741.1

Kim H, Vitart F, Waliser DE (2018) Prediction of the Madden–Julian Oscillation: a review. J Clim 31:9425–9443. https://doi.org/10.1175/JCLI-D-18-0210.1

Knippertz P, Todd MC (2010) The central west Saharan dust hot spot and its relation to African easterly waves and extratropical disturbances. J Geophys Res Atmos, https://doi.org/10.1029/2009JD012819

Lafore J-P, Coauthors (2017) A multi-scale analysis of the extreme rain event of Ouagadougou in 2009. Q J R Meteorol Soc 143:3094–3109. https://doi.org/10.1002/qj.3165

Largeron Y, Guichard F, Roehrig R, Couvreux F, Barbier J (2020) The April 2010 North African heatwave: when the water vapor greenhouse effect drives nighttime temperatures. Clim Dyn 54:3879–3905. https://doi.org/10.1007/s00382-020-05204-7

Lavaysse C, Flamant C, Janicot S, Parker DJ, Lafore J-P, Sultan B, Pelon J (2009) Seasonal evolution of the West African heat low: a climatological perspective. Clim Dyn 33:313–330. https://doi.org/10.1007/s00382-009-0553-4

Lavender SL, Matthews AJ (2009) Response of the West African Monsoon to the Madden–Julian Oscillation. J Clim 22:4097–4116. https://doi.org/10.1175/2009JCLI2773.1

Li Y, Stechmann SN (2020) Predictability of tropical rainfall and waves: estimates from observational data. Q J R Meteorol Soc 146:1668–1684. https://doi.org/10.1002/qj.3759

Lothon M, Saïd F, Lohou F, Campistron B (2008) Observation of the diurnal cycle in the low troposphere of West Africa. Mon Wea Rev 136:3477–3500. https://doi.org/10.1175/2008MWR2427.1

Liebmann B, Smith CA (1996) Description of a Complete (Interpolated) Outgoing Longwave Radiation Dataset. Bull Am Meteorol Soc 77:1275–1277

Madden RA (1994) Observations of the 40–50-Day Tropical Oscillation—a review. Mon Weather Rev 122:814–837.https://doi.org/10.1175/1520-0493(1994)122<0814:OOTDTO>2.0.CO;2

Madden RA, Julian PR (1971) Detection of a 40–50 Day Oscillation in the Zonal Wind in the Tropical Pacific. J Atmos Sci 28:702–708. https://doi.org/10.1175/1520-0469(1971)028<0702:DOADOI>2.0.CO;2

Madden RA, Julian PR (1972) Description of global-scale circulation cells in the tropics with a 40–50 day period. J Atmos Sci 29:1109–1123. https://doi.org/10.1175/1520-0469(1972)029<1109:DOGSCC>2.0.CO;2

Martens B, Schumacher DL, Wouters H, Muñoz-Sabater J, Verhoest NEC, Miralles DG (2020) Evaluating the surface energy partitioning in ERA5. Geoscientific Model Development Discussions, 1–35, https://doi.org/10.5194/gmd-2019-315

Mazdiyasni O, AghaKouchak A (2015) Substantial increase in concurrent droughts and heatwaves in the United States. Proc Natl Acad Sci USA 112:11484–11489. https://doi.org/10.1073/pnas.1422945112

Mekonnen A, Thorncroft CD, Aiyyer AR, Kiladis GN (2008) Convectively coupled kelvin waves over Tropical Africa during the boreal summer: structure and variabilityy. J Clim 21:6649–6667. https://doi.org/10.1175/2008JCLI2008.1

Mera R, Laing AG, Semazzi F (2014) Moisture variability and multiscale interactions during spring in West Africa. Mon Weather Rev 142:3178–3198. https://doi.org/10.1175/MWR-D-13-00175.1

Moron V, Oueslati B, Pohl B, Janicot S (2018a) Daily Weather Types in February–June (1979–2016) and Temperature Variations in Tropical North Africa. J Appl Meteorol Climatol 57:1171–1195. https://doi.org/10.1175/JAMC-D-17-0105.1

Moron V, Oueslati B, Pohl B, Rome S, Janicot S (2016) Trends of mean temperatures and warm extremes in northern tropical Africa (1961–2014) from observed and PPCA-reconstructed time series. J Geophys Res Atmos 121:5298–5319. https://doi.org/10.1002/2015JD024303

Moron AW, Robertson, Vitart F (2018b) Editorial: Sub-seasonal to Seasonal Predictability and Prediction of Monsoon Climates. Front Environ Sci, 6, https://doi.org/10.3389/fenvs.2018.00083

Murage P, Hajat S, Kovats RS (2017) Effect of night-time temperatures on cause and age-specific mortality in London. Environ Epidemiol 1:e005. https://doi.org/10.1097/EE9.0000000000000005

Murari KK, Sahana AS, Daly E, Ghosh S (2016) The influence of the El Niño Southern Oscillation on heat waves in India. Meteorol Appl 23:705–713. https://doi.org/10.1002/met.1594

Nguyen H, Thorncroft CD, Zhang C (2011) Guinean coastal rainfall of the West African Monsoon. Q J R Meteorol Soc 137:1828–1840. https://doi.org/10.1002/qj.867

Nicholson SE (2018) Climate of the Sahel and West Africa. Oxford Research Encyclopedia of Climate Science. https://doi.org/10.1093/acrefore/9780190228620.013.510

Nissan H, Burkart K, Coughlan de Perez E et al (2017) Defining and Predicting Heat Waves in Bangladesh. J Appl Meteorol Climatol 56:2653–2670. https://doi.org/10.1175/JAMC-D-17-0035.1

Olauson J (2018) ERA5: the new champion of wind power modelling? Renew Energy 126:322–331. https://doi.org/10.1016/j.renene.2018.03.056

Oueslati B, Pohl B, Moron V, Rome S, Janicot S (2017) Characterization of heat waves in the Sahel and associated physical mechanisms. J Clim 30:3095–3115. https://doi.org/10.1175/JCLI-D-16-0432.1

Parker TJ, Berry GJ, Reeder MJ, Nicholls N (2014) Modes of climate variability and heat waves in Victoria, southeastern Australia. Geophys Res Lett 41:6926–6934. https://doi.org/10.1002/2014GL061736

Pearson KJ, Hogan RJ, Allan RP et al (2010) Evaluation of the model representation of the evolution of convective systems using satellite observations of outgoing longwave radiation. J Geophys Res Atmos 115: https://doi.org/10.1029/2010JD014265

Perkins SE (2015) A review on the scientific understanding of heatwaves—Their measurement, driving mechanisms, and changes at the global scale. Atmos Res 164–165:242–267. https://doi.org/10.1016/j.atmosres.2015.05.014

Ramon J, Lledó L, Torralba V, Soret A, Doblas-Reyes FJ (2019) What global reanalysis best represents near-surface winds? Q J R Meteorol Soc 145:3236–3251. https://doi.org/10.1002/qj.3616

Raymond C, Matthews T, Horton RM (2020) The emergence of heat and humidity too severe for human tolerance. Sci Adv 6:eaaw1838. https://doi.org/10.1126/sciadv.aaw1838

Riley EM, Mapes BE, Tulich SN (2011) Clouds Associated with the Madden–Julian Oscillation: A New Perspective from CloudSat. J Atmos Sci 68:3032–3051. https://doi.org/10.1175/JAS-D-11-030.1

Ringard J, Coauthors (2016) The intensification of thermal extremes in west Africa. Global Planet Change, 139, 66–77, https://doi.org/10.1016/j.gloplacha.2015.12.009

Russo S, Marchese AF, Sillmann J, Immé G (2016) When will unusual heat waves become normal in a warming Africa? Environ Res Lett 11:054016. https://doi.org/10.1088/1748-9326/11/5/054016

Russo S, Dosio A, Graversen RG et al (2014) Magnitude of extreme heat waves in present climate and their projection in a warming world. Journal of Geophysical Research: Atmospheres 119:12,500 – 12,512. https://doi.org/10.1002/2014JD022098

Schamm K, Ziese M, Becker A, Finger P, Meyer-Christoffer A, Schneider U, Schröder M, Stender P (2014) Global gridded precipitation over land: a description of the new GPCC First Guess Daily product. Earth Syst Sci Data 6:49–60. https://doi.org/10.5194/essd-6-49-2014

Schlueter A, Fink AH, Knippertz P (2019b) A Systematic Comparison of Tropical Waves over Northern Africa. Part II: Dynamics and Thermodynamics. J Clim 32:2605–2625. https://doi.org/10.1175/JCLI-D-18-0651.1

Schlueter A, Fink AH, Knippertz P, Vogel P (2019a) A Systematic Comparison of Tropical Waves over Northern Africa. Part I: Influence on Rainfall. J Clim 32:1501–1523. https://doi.org/10.1175/JCLI-D-18-0173.1

Schreck CJ, Mohr KI (2011) Attributing Tropical Cyclogenesis to Equatorial Waves in the Western North Pacific. J Atmos Sci 68:195–209. https://doi.org/10.1175/2010JAS3396.1

Schreck CJ, Molinari J (2011) Tropical Cyclogenesis Associated with Kelvin Waves and the Madden–Julian Oscillation. Mon Weather Rev 139:2723–2734. https://doi.org/10.1175/MWR-D-10-05060.1

Schär C (2016) The worst heat waves to come. Nat Clim Change 6:128–129. https://doi.org/10.1038/nclimate2864

Slingo A, White HE, Bharmal NA, Robinson GJ (2009) Overview of observations from the RADAGAST experiment in Niamey, Niger: 2. Radiative fluxes and divergences. J Geophys Res Atmos, 114, https://doi.org/10.1029/2008JD010497

Song E-J, Seo K-H (2016) Past- and present-day Madden-Julian Oscillation in CNRM-CM5. Geophys Res Lett 43:4042–4048. https://doi.org/10.1002/2016GL068771

Sossa A, Liebmann B, Bladé I, Allured D, Hendon HH, Peterson P, Hoell A (2017) Statistical Connection between the Madden–Julian Oscillation and Large Daily Precipitation Events in West Africa. J Clim 30:1999–2010. https://doi.org/10.1175/JCLI-D-16-0144.1

Straub KH, Kiladis GN (2002) Observations of a Convectively Coupled Kelvin Wave in the Eastern Pacific ITCZ. J Atmos Sci 59:30–53. https://doi.org/10.1175/1520-0469(2002)059<0030:OOACCK>2.0.CO;2

Tall M, Albergel C, Bonan B et al (2019) Towards a Long-Term Reanalysis of Land Surface Variables over Western Africa: LDAS-Monde Applied over Burkina Faso from 2001 to 2018. Remote Sens 11:735. https://doi.org/10.3390/rs11060735

Tschakert P (2007) Views from the vulnerable: Understanding climatic and other stressors in the Sahel. Glob Environ Change 17:381–396. https://doi.org/10.1016/j.gloenvcha.2006.11.008

Ventrice MJ, Thorncroft CD (2012) The Role of Convectively Coupled Atmospheric Kelvin Waves on African Easterly Wave Activity. Mon Weather Rev 141:1910–1924. https://doi.org/10.1175/MWR-D-12-00147.1

Wang Y, Notaro M, Liu Z, Gallimore R, Levis S, Kutzbach JE (2008) Detecting vegetation-precipitation feedbacks in mid-Holocene North Africa from two climate models. Clim Past 4:59–67. https://doi.org/10.5194/cp-4-59-2008

Wang H, Loeb NG, Su W, Rose FG, Kato S, Doelling DR (2017) Evaluating Radiative Fluxes in Current Reanalyses using CERES EBAF-TOA and EBAF-Surface Ed4.0. 23. Presented at the Fall 2017 CERES Science Team Meeting, September 2017. https://ceres.larc.nasa.gov/documents/STM/2017-09/23_CERES_Fall2017_HailanWang.WedesdayPM.pdf

Wheeler M, Kiladis GN (1999) Convectively Coupled Equatorial Waves: Analysis of Clouds and Temperature in the Wavenumber–Frequency Domain. J Atmos Sci 56:374–399. https://doi.org/10.1175/1520-0469(1999)056<0374:CCEWAO>2.0.CO;2

Wheeler MC, Nguyen H (2015) TROPICAL METEOROLOGY AND CLIMATE | Equatorial Waves. In: North GR, Pyle J, Zhang F (eds) Encyclopedia of Atmospheric Sciences (Second Edition). Academic Press, Oxford, pp 102–112

Wielicki, B. A., B. R. Barkstrom, E. F. Harrison, R. B. Lee, G. L. Smith, and J. E. Cooper, 1996: Clouds and the Earth's Radiant Energy System (CERES): An Earth Observing System Experiment. Bull Am Meteorol Soc, 77, 853–868, https://doi.org/10.1175/1520-0477(1996)077<0853:CATERE>2.0.CO;2

Wilkinson E, Weingärtner L, Choularton R, Bailey M, Todd M, Kniveton D, Cabot Venton C (2018) Forecasting hazards, averting disasters: implementing forecast-based early action at scale. Overseas Development Institute (ODI), http://lib.riskreductionafrica.org/handle/123456789/1501. Accessed 3 Jan 2019

World Meteorological Organization and World Health Organization (2015) Heatwaves and Health: Guidance on Warning-System Development. WMO-No. 1142, Geneva

Wright JS, Sun X, Konopka P et al (2020) Differences in tropical high clouds among reanalyses: origins and radiative impacts. Atmos Chem Phys 20:8989–9030. https://doi.org/10.5194/acp-20-8989-2020

Xavier P, Rahmat R, Cheong WK, Wallace E (2014) Influence of Madden-Julian Oscillation on Southeast Asia rainfall extremes: Observations and predictability. Geophys Res Lett 41:4406–4412. https://doi.org/10.1002/2014GL060241

Xu C, Kohler TA, Lenton TM, Svenning J-C, Scheffer M (2020) Future of the human climate niche. PNAS. https://doi.org/10.1073/pnas.1910114117

Yang G-Y, Methven J, Woolnough S, Hodges K, Hoskins B (2018) Linking African Easterly Wave Activity with Equatorial Waves and the Influence of Rossby Waves from the Southern Hemisphere. J Atmos Sci 75:1783–1809. https://doi.org/10.1175/JAS-D-17-0184.1